

Accuracy of Planar Dosimetry for Volumetric  
Modulated Arc Therapy Quality Assurance

by

Monica Kishore

Medical Physics Graduate Program  
Duke University

Date: \_\_\_\_\_

Approved:

\_\_\_\_\_  
Jennifer O'Daniel, Co-Supervisor

\_\_\_\_\_  
Fang-Fang Yin, Co-Supervisor

\_\_\_\_\_  
James Bowsher

\_\_\_\_\_  
Robert Reiman

Thesis submitted in partial fulfillment of the requirements for the degree of  
Master of Science in the Medical Physics Graduate Program  
in the Graduate School of Duke University  
2011

ABSTRACT

Accuracy of Planar Dosimetry for Volumetric Modulated Arc  
Therapy Quality Assurance

by

Monica Kishore

Medical Physics Graduate Program  
Duke University

Date: \_\_\_\_\_

Approved:

---

Jennifer O'Daniel, Co-Supervisor

---

Fang-Fang Yin, Co-Supervisor

---

James Bowsher

---

Robert Reiman

An abstract of a thesis submitted in partial fulfillment of the requirements for  
the degree of Master of Science in the Medical Physics Graduate Program  
in the Graduate School of Duke University  
2011

Copyright © 2011 by Monica Kishore  
All rights reserved

# Abstract

With the advent of new, more efficient, rotational therapy techniques such as volumetric modulated arc therapy (VMAT), radiation therapy treatment precision requires evolving quality assurance. Two dimensional (2D) detector arrays have shown angular dependence that must be compensated for by the creation of angular correction factor tables. Currently available correction factor tables have several underlying assumptions that leave room for improvement: first, these correction factors assume that the response of all ion chambers is identical for each angle; second, that the ion chamber array response from gantry angles  $0^\circ - 180^\circ$  are equivalent to the response from  $180^\circ - 360^\circ$ ; and, third, that the response is independent of the direction of rotation.

Measurements were acquired using a 2D ion chamber array (MatriXX<sup>®</sup>, IBA Dosimetry) for static open fields delivered every  $5^\circ$  around the MatriXX while dose was calculated using Eclipse v8.6 (analytic anisotropic algorithm, Varian Medical Systems). Customized correction factors were created by dividing the calculated dose by the measured dose for each ion chamber. Two measurement positions were used in the creation of the custom correction factors: a coronal position in which the couch was included, and two sagittal orientations in which the couch was not included.

The correction factors were verified using open field arcs and VMAT patient plans, where measured doses were compared to calculated doses using gamma analysis (3%,

3 mm). Narrow fields were also delivered clockwise and counterclockwise in order to investigate the effect of the internal structure of the ion chamber array.

The angular response of the individual ion chambers appears to vary significantly ( $1 \sigma \leq 4.6\%$ ). The response from  $0^\circ - 180^\circ$  vs  $180^\circ - 360^\circ$  is significantly different (paired t-test yields  $p < 0.0001$ ). Custom correction factors do enhance the agreement between measured and calculated doses for open field arcs and VMAT patient plans compared to the default correction factors. The direction of rotation appears to affect the dose to the penumbra region of narrow fields, which could affect VMAT patient specific quality assurance.

The custom correction factor tables, using measurements for individual ion chambers over a full  $0^\circ - 360^\circ$  range, allows for improved accuracy in measurements by the 2D ion chamber array. However, even the corrected measurements still showed discrepancies with the calculated doses for VMAT plans.

# Contents

<b>Abstract</b>	<b>iv</b>
<b>List of Tables</b>	<b>ix</b>
<b>List of Figures</b>	<b>xi</b>
<b>Acknowledgements</b>	<b>xiii</b>
<b>1 Introduction</b>	<b>1</b>
<b>2 Background</b>	<b>2</b>
2.1 Three Dimensional Conformal Radiation Therapy . . . . .	2
2.2 Intensity Modulated Radiation Therapy . . . . .	3
2.3 Volumetric Modulated Arc Therapy . . . . .	5
2.4 Patient Specific Quality Assurance of IMAT Plans . . . . .	7
2.5 MatriXX Evolution . . . . .	15
2.5.1 Clinical Verification of the MatriXX . . . . .	18
2.5.2 Evaluation of the MatriXX Device in Patient-Specific IMRT Verification. . . . .	19
2.5.3 Investigation of Angular Dependent Response . . . . .	20
2.6 Aims . . . . .	24
<b>3 Methods and Materials</b>	<b>26</b>
3.1 Equipment . . . . .	26
3.1.1 MatriXX Treatment Planning and Set-up . . . . .	26

3.1.2	Measurements . . . . .	27
3.2	ICA Evaluation . . . . .	28
3.2.1	Consistency . . . . .	28
3.3	Intrinsic MatriXX Response . . . . .	29
3.3.1	Counterclockwise vs. Clockwise: Open Field Stationary Angles	29
3.3.2	Counterclockwise vs. Clockwise: Open Field Arcs . . . . .	29
3.3.3	Counterclockwise vs. Clockwise: Small Field Arcs . . . . .	30
3.3.4	MLC Sliding Window Static Gantry . . . . .	30
3.4	Creation of Angle Dependent Correction Factors . . . . .	31
3.4.1	Measurement Data . . . . .	31
3.4.2	Eclipse Calculations . . . . .	31
3.4.3	MATLAB . . . . .	32
3.4.4	Statistical Analysis using Paired T-Test . . . . .	32
3.4.5	Smoothing . . . . .	33
3.5	Correction Factor Analysis . . . . .	34
3.5.1	Correction Factor Measurement Consistency . . . . .	34
3.5.2	Correction Factor Asymmetry . . . . .	34
3.6	CF Verification . . . . .	34
3.6.1	Open Arcs . . . . .	35
3.6.2	Patient Plans . . . . .	35
<b>4</b>	<b>Results</b>	<b>37</b>
4.1	ICA Consistency . . . . .	37
4.2	Intrinsic MatriXX Response . . . . .	37
4.2.1	Counterclockwise vs. Clockwise: Open Field Stationary Angles	37
4.2.2	Counterclockwise vs. Clockwise: Open Field Arcs . . . . .	37

4.2.3	Counterclockwise vs. Clockwise: Small Field Arcs . . . . .	38
4.2.4	MLC Sliding Window Static Gantry . . . . .	38
4.3	Correction Factor Analysis . . . . .	38
4.3.1	Correction Factor Measurement Consistency . . . . .	38
4.3.2	Correction Factor Asymmetry . . . . .	40
4.4	CF Verification . . . . .	43
4.4.1	Open Arcs . . . . .	43
4.4.2	Patient Plans . . . . .	43
<b>5</b>	<b>Discussion</b>	<b>52</b>
5.1	ICA Consistency . . . . .	52
5.2	Intrinsic MatriXX Response . . . . .	52
5.3	Correction Factor Analysis . . . . .	55
5.4	CF Verification . . . . .	57
<b>6</b>	<b>Conclusion</b>	<b>59</b>
<b>A</b>	<b>Generation of Correction Factors</b>	<b>60</b>
A.1	Steps for Creating a Correction Factor File . . . . .	60
A.2	Rename Dicom Code . . . . .	64
A.3	Coronal Correction Factor Code . . . . .	65
A.4	Sagittal Correction Factor Code . . . . .	72
A.4.1	Sagittal270 Correction Factor Code . . . . .	76
A.4.2	Sagittal90 Correction Factor Code . . . . .	80
	<b>Bibliography</b>	<b>85</b>

# List of Tables

3.1	Open field partial arcs subtending angles of $45^\circ$ and $90^\circ$ , and the respective number of monitor units delivered to achieve $2.22 \frac{MU}{\circ}$ . . .	30
4.1	The average and standard deviation of the left and right side ion chamber measurements given as a percentage of the maximum value of both sides for 6 MV and 15 MV small fields. . . . .	41
4.2	The results for 6 MV and 15 MV MLC sliding window static fields are given as the percent of pixels passing a gamma analysis. . . . .	41
4.3	The gantry angles at which the standard deviation $\sigma > 0.03$ of the correction factors are given for 6 MV coronal and sagittal and 15 MV coronal and sagittal. . . . .	44
4.4	CF verification results for 6 MV open fields delivered CCW. The percent of pixels passing a gamma analysis are given when no correction factor is used, when the two manufacturer correction factors are used, and when the two custom correction factors are used on the doses measured by the ICA. N.B. Data collected without background subtraction. . . . .	49
4.5	CF verification results for 6 MV open fields delivered CW. The percent of pixels passing a gamma analysis are given when no correction factor is used, when the two manufacturer correction factors are used, and when the two custom correction factors are used on the doses measured by the ICA. . . . .	49
4.6	CF verification results for 15 MV open fields delivered CCW. The percent of pixels passing a gamma analysis are given when no correction factor is used, when the two manufacturer correction factors are used, and when the two custom correction factors are used on the doses measured by the ICA. . . . .	50

4.7	CF verification results for 15 MV open fields delivered CW. The percent of pixels passing a gamma analysis are given when no correction factor is used, when the two manufacturer correction factors are used, and when the two custom correction factors are used on the doses measured by the ICA. . . . .	50
4.8	CF verification results for three 6 MV patient plans. The percent of pixels passing a gamma analysis are given when no correction factor is used, when the two manufacturer correction factors are used, and when the two custom correction factors are used on the doses measured by the ICA. N.B. Data gathered without forcing agreement of Eclipse and measurement. . . . .	51
4.9	CF verification results for two 15 MV patient plans. The percent of pixels passing a gamma analysis are given when no correction factor is used, when the two manufacturer correction factors are used, and when the two custom correction factors are used on the doses measured by the ICA. . . . .	51

# List of Figures

2.1	1 Monitor Unit corresponds to the machine output required to deliver 1 cGy at reference conditions. The reference conditions are given as a source-to-surface distance of 100 cm and depth $d_{\max}$ , where $d_{\max}$ is the beam energy dependent depth at which the maximum dose will be delivered. The field size is usually $10 \times 10 \text{ cm}^2$ at reference conditions.	5
3.1	The ICA is shown positioned on the couch in the coronal position. . .	27
3.2	The diagram shows the general connections between the ICA, the power supply, gantry angle sensor and the PC. . . . .	28
3.3	(a) Sagittal90 Orientation: Measurement includes gantry angles $270^\circ - 0^\circ - 90^\circ$ . The red dotted line indicates the plane of ion chambers facing gantry angle $90^\circ$ with the blue line indicating a plane of high density material. (b) Sagittal270 Orientation: Measurement includes gantry angles $270^\circ - 0^\circ - 90^\circ$ . The red dotted line indicates the plane of ion chambers facing gantry angle $270^\circ$ with the blue line indicating a plane of high density material.(c) Using the combination of two sagittal measurements creates a new $360^\circ$ measurement without the effect of couch attenuation. Alternatively, a $360^\circ$ measurement can also be created with the ICA in the coronal orientation and which does include the effect of the couch in measurements. . . . .	36
4.1	6 MV CCW-CW difference map. . . . .	39
4.2	15 MV CCW-CW difference map. . . . .	39
4.3	6x coronal CF mean and standard deviation. . . . .	41
4.4	15x coronal CF mean and standard deviation. . . . .	42
4.5	6x sagittal CF mean and standard deviation. . . . .	42
4.6	15x sagittal CF mean and standard deviation. . . . .	44

4.7	6x coronal set-up average and standard deviation of CF for mirrored angles. Gantry angle $90^\circ$ of CF $0 - 180^\circ$ corresponds to gantry angle $270^\circ$ for CF $180 - 360^\circ$ . . . . .	45
4.8	15x coronal set-up average and standard deviation of CF for mirrored angles. Gantry angle $90^\circ$ of CF $0 - 180^\circ$ corresponds to gantry angle $270^\circ$ for CF $180 - 360^\circ$ . . . . .	45
4.9	6x sagittal set-up average and standard deviation of CF for mirrored angles. Gantry angle $90^\circ$ of CF $0 - 180^\circ$ corresponds to gantry angle $270^\circ$ for CF $180 - 360^\circ$ . . . . .	46
4.10	15x sagittal set-up average and standard deviation of CF for mirrored angles. Gantry angle $90^\circ$ of CF $0 - 180^\circ$ corresponds to gantry angle $270^\circ$ for CF $180 - 360^\circ$ . . . . .	46
4.11	6x coronal: At each gantry angle, the ratio of the average of 1024 correction factors to the four central axis (CAX) correction factors is given and the standard deviation for the 6 MV coronal correction factor.	47
4.12	15x coronal: At each gantry angle, the ratio of the average of 1024 correction factors to the four central axis (CAX) correction factors is given and the standard deviation for the 15 MV coronal correction factor . . . . .	47
4.13	6x sagittal: At each gantry angle, the ratio of the average of 1024 correction factors to the four central axis (CAX) correction factors is given and the standard deviation for the 6 MV sagittal correction factor	48
4.14	15x sagittal: At each gantry angle, the ratio of the average of 1024 correction factors to the four central axis (CAX) correction factors is given and the standard deviation for the 15 MV sagittal correction factor . . . . .	48
5.1	CT scan of ICA showing plane of ion chambers and high density material plane below. . . . .	54

# Acknowledgements

I would like to thank my advisor, Dr. Jennifer O'Daniel, for making this project possible and for her continued guidance and encouragement. I would also like to thank Dr. Fang-Fang Yin for his advice and support. I am grateful to the members of my thesis committee, Dr. James Bowsher and Dr. Robert Reiman for serving on my committee and providing useful suggestions to improve my project. Lastly, I would like to thank my family and friends for their support throughout this project.

# 1

## Introduction

The outcome of radiation therapy treatment relies on the accurate delivery of radiation to approximately  $\pm 5\%$  of the prescribed dose[1]. Machine and patient-specific quality assurance utilizes appropriate equipment to ensure the effective delivery of radiation within this margin of accuracy. With the advent of volumetric modulated arc therapy (VMAT), the increased complexity of the treatment delivery may require new quality assurance methods and equipment. A background of the development and features of VMAT will be presented. The devices available for quality assurance are discussed within the context of VMAT requirements. Finally, the aim of this project and its significance are presented.

# 2

## Background

### 2.1 Three Dimensional Conformal Radiation Therapy

3D conformal radiation therapy (3D-CRT) represents a volumetric, image-based approach to defining individual patient treatment plans. Typically, a patient is immobilized in his or her treatment position and imaged using a 3D computed tomography (CT) scan, after which critical normal structures and target volumes are contoured to create a 3D data set. Beam orientation and custom blocking using block apertures or multi-leaf collimator (MLC) settings are chosen[2]. The planning process includes accurate delineation of target and relevant anatomic structures, field arrangement, and optimization of the dose distribution in accordance with clinical objectives[1].

The ability of 3D-CRT to achieve treatment objectives is constrained by the patient's anatomy, which determines beam orientation and blocking depending on the location of the tumor and nearby critical structures. While there are limits to 3D-CRT therapy, overall the therapy seems to offer an improvement over 2D conventional therapy because increasing accuracy in patient positioning has resulted in the ability to reduce margins, making a favorable therapeutic outcome more likely as the dose to

normal tissue is reduced. As further improvements in delivery have been defined by even greater conformity to achieve better patient outcomes, dosimetric verification becomes even more necessary.

## 2.2 Intensity Modulated Radiation Therapy

In the past decade, improvements in image-guided positioning, plan adaptation, and optimization have resulted in the advent of intensity-modulated radiation therapy (IMRT). IMRT treats patients from different directions with beams of nonuniform fluences. The beams are optimized to deliver a high dose to the target volume and low dose to the surrounding normal tissue. The treatment planning system breaks the radiation field at each gantry angle into a large number of beamlets and determines their optimum weighting to achieve a pre-defined dose distribution in a process known as inverse planning. Optimum beamlet intensities are determined iteratively, with the treatment planning system evaluating each successive dose distribution according to user determined objectives. Incremental changes in individual beamlet intensities are made as a result of the deviation from objectives[1, 2]. The ability to manipulate individual beamlets allows for even greater customization of dose distribution compared to 3D-CRT and may lead to an improved therapeutic ratio[2, 3, 4].

IMRT has the advantage of better conformity for complex-shaped target volumes and lower doses to nearby organs-at-risk than 3D-CRT, which may result in a better clinical outcome[5]. Dose distributions within the PTV can be more homogeneous and have a sharper fall-off of dose at the boundary than 3D-CRT, although inhomogeneity is often observed due to competing objectives which require the protection of normal tissue structures while also delivering the prescribed dose to the target volume. With the possibility of a sharper dose fall-off at the boundary of the PTV, the volume of normal tissue that is exposed to high doses can be reduced in comparison

to 3D-CRT, enabling the possibility of tumor dose escalation.

Limitations to both 3D-CRT and IMRT include having an accurate knowledge of the tumor extent, changes in inter-fraction and intra-fraction patient position, beam penumbra, and changes in radiobiologic characteristics of tumors and normal tissue. Despite advances in imaging technology, there remains uncertainty in localization of the clinical target volume which includes the microscopic spread of disease. While 3D-CRT and IMRT increase conformity of the beam, the reduced margins also increase the risk of missing the target due to limits of target localization or errors in patient set-up. Beam penumbra, a region of steep dose gradient at the edge of the field, places further requirements on uniform irradiation of the planning target volume (PTV). Similarly, the varied biologic response of tumor and normal tissue complicate the optimization of the plan. Biological limits depend on disease characteristics and normal tissue response. The endpoint for optimization of biological response must balance tumor control with the likelihood of normal tissue complication, but clinical data to support models of tissue and tumor response are scarce. As well, radiation scattering and transmission through the MLC leaves and limits to dose-calculation models constrain the accuracy and ability to deliver the planned fluence distribution. The limits and risks associated with 3D-CRT and IMRT require further efforts to improve planning, delivery, and verification of delivered dose[1, 2].

While in theory IMRT has the potential to surpass 3D-CRT in terms of controlling the dose distribution to fit the tumor and spare nearby critical structures, it also has some unique detractors. These include a lengthened beam delivery time when compared to 3D-CRT, leading to an increased risk of intra-fractional patient motion[6]. IMRT can also require longer treatment times than 3D-CRT, increasing the amount of secondary radiation received due to the scattering of primary radiation within the patient and by leakage of radiation from the gantry head, in turn increasing the possibility of secondary malignancies[7]. Lengthened treatment times

are often associated with an increased number of monitor units, where one monitor unit (MU) represents the machine output required to deliver 1 cGy at calibration set-up (See Figure 2.1). Finally, patient throughput may also be reduced due to the increased time required for treatment delivery[8].

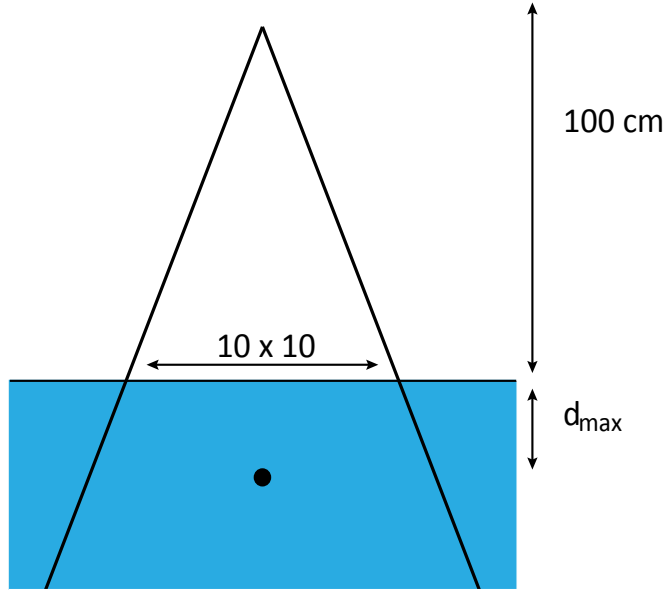


FIGURE 2.1: 1 Monitor Unit corresponds to the machine output required to deliver 1 cGy at reference conditions. The reference conditions are given as a source-to-surface distance of 100 cm and depth  $d_{\max}$ , where  $d_{\max}$  is the beam energy dependent depth at which the maximum dose will be delivered. The field size is usually  $10 \times 10 \text{ cm}^2$  at reference conditions.

### 2.3 Volumetric Modulated Arc Therapy

Volumetric modulated arc therapy (VMAT) is a subset of IMRT that fully utilizes the advantages of having an increased number of beam directions by allowing arc based delivery. Prior to VMAT, intensity-modulated arc therapy (IMAT) was proposed by Yu[9]. IMAT allowed for beam delivery with continuous MLC movement while rotating the gantry. Linear accelerators were not capable of dose rate modulation during delivery at the time that IMAT was proposed, which resulted in an under-

lying assumption that arcs could only be delivered with constant dose rates. The constraints that were placed on the multi-leaf collimators (MLCs) between gantry positions lead to the need for multiple arcs which resulted in treatment times on the same order as those of IMRT treatments, and made clinical implementation slow to follow. In order to realize the potential of IMAT, Otto[10] proposed VMAT, a new form of IMAT optimization where treatment is delivered in a single intensity modulated arc[10].

With VMAT, three dynamic parameters, dose rate, beam aperture shape, and the speed of rotation, can be continuously varied to deliver the prescribed dose to the planning target volume while sparing the organs-at-risk and normal tissue. The MLC shapes and weights are initially optimized for a coarse sampling of beam angles, with minimal consideration for connectivity between shapes. By disregarding the MLC connectivity initially, the optimization focuses on obtaining an optimal dose distribution with the flexibility to allow large MLC displacements and MU weight changes. As the algorithm converges, the number of beam angles sampled increases, and as the angular spacing becomes small the optimization gives greater consideration to the connectivity of aperture shape between consecutive beam angles. Eventually, the MLC positions of the newly inserted beam angles are linearly interpolated from their neighboring aperture shapes. The overall process of coarse-to-fine sampling is known as progressive sampling and allows for a speedy optimization[10].

VMAT constraints only allow physically achievable MLC positions and MU values, such that overlapping leaves or negative MU weights are impossible. Efficiency constraints are also used when the system takes into account the need for continuous delivery, constraining the maximum leaf displacement so that the total time for MLC motion over a full arc matches the total time for gantry rotation and also constraining the MU weights which would exceed the maximum dose rate to be deliverable by reducing gantry rotation speed. Since it is undesirable to reduce gantry speed be-

cause it will increase the delivery time and may result in a less accurate delivery, the optimization algorithm preferentially maximizes dose rate over slowing down gantry rotation. In order to maximize dosimetric accuracy and optimize the time required with fixed sampling, gantry angle and MLC spacing as low as  $1^\circ$  and 0.5 cm, respectively, are the most desirable for accurate and efficient dose modeling. Otto has indicated that a 200 cGy fraction can be delivered in 1.5 – 3 min using the VMAT technique[10] and subsequent studies have indeed found that VMAT uses both fewer MU's and a shorter treatment time than IMRT while still achieving favorable dose distributions[11, 12, 13].

## 2.4 Patient Specific Quality Assurance of IMAT Plans

The American Association of Physicists in Medicine (AAPM), the American Society for Therapeutic Radiology and Oncology (ASTRO), and the American College of Radiology (ACR) recommend patient-specific quality assurance (QA) for IMRT treatments to verify the actual radiation dose being received during treatment delivery[14, 15]. This verification should occur before the start of treatment by irradiating an independently calibrated dosimetry system. Documentation of the agreement between planned and delivered dose should be maintained for each patient[15]. Implementation of patient-specific quality assurance is strongly recommended because of the complexity of irregular field shapes, small-field dosimetry and time-dependent leaf sequences. It is also required as a prerequisite for billing of IMRT services[2].

Although a variety of devices exist which can measure dosimetric data, it is the comparison of measured versus calculated dose distribution that is essential for QA. Comparison can be made by superimposing isodose distributions or analyzing the agreement of line profiles, but both of these methods are manual and therefore time consuming, relying on the experience of the physicist for accurate assessment[16].

Quantitative analysis of two dimensional dose distributions often makes use of the method presented by Low et al.[17], which is known as the gamma method. This method is designed to compare two dose distributions in a single composite measure based on both dose and spatial domains. The gamma method uses dose and spatial acceptance tolerances which are usually presented in terms of percent dose difference and distance-to-agreement (DTA) respectively, as shown in equation 2.1

$$\sqrt{\left(\frac{\Delta d}{\Delta d_t}\right)^2 + \left(\frac{\Delta D}{\Delta D_t}\right)^2} \leq 1 \quad (2.1)$$

where, for a reference location, equation 2.1 is evaluated at all points with  $\Delta D$  as the dose difference and  $\Delta d$  as the distance shift to the point evaluated.  $\Delta D_t$  and  $\Delta d_t$  are the tolerances for error, e.g. 3% and 3 mm. Based on the evaluation of equation 2.1, a numerical index,  $\gamma$ , provides a pass fail criteria as shown in equation 2.2

$$\gamma = \min \left( \sqrt{\left(\frac{\Delta d}{\Delta d_t}\right)^2 + \left(\frac{\Delta D}{\Delta D_t}\right)^2} \right) \quad (2.2)$$

where  $\gamma \geq 1$  corresponds to locations where the dose distribution fails to meet the acceptance criteria[17].

VMAT, as an extension of dynamic multi-leaf collimator IMRT, requires quality assurance that is even more intensive than that of IMRT. The increased functionality of VMAT, due to the incorporation of variable dose rate, variable gantry speed and dynamic MLC during gantry rotation, results in additional uncertainties which must be investigated[18]. Initial commissioning and QA protocols have been described by Ling et al.[19] and Bedford et al.[20]. Such protocols address the accuracy of MLC position, variable dose rate, and MLC leaf speed, as well as tests for beam flatness and symmetry at variable dose rates[19, 20]. However, additional measurements are required for patient-specific dosimetry[19].

Initial efforts at VMAT patient-specific QA have adapted some techniques from patient-specific QA of static IMRT[18], using a variety of techniques and equipment[21, 22, 23, 24, 25, 26, 27].

Schreibmann et al.[21] assessed the accuracy of VMAT plans using the dynamic multi-leaf collimator (DMLC) and treatment controller log files for five prostate patients. Values were recorded in log files for gantry angle and dose rate at each segment of the arc (designated by a set of control points), and for leaf positions at 50 ms intervals during treatment. Using the planned treatment DICOM file, which consisted of leaf position, gantry angle, and cumulative dose for each of 177 control points of the RapidArc plan, the values recorded in the log files were converted to a new plan using in-house software. The software created by Schreibmann et al. took the corresponding recorded values from the log files and input the values into the DICOM file, creating a new plan. This new plan, known as the reconstructed dose distribution, was compared to the original plan, referred to as the planned dose distribution, using dose-volume histograms of the dose from both plans to evaluate coverage. Additionally, spatial evaluation used a composite plan that was created by subtracting one dose distribution from the other. A 2D dosimeter array was used for the initial verification of this method. Schreibmann et al. found that this method of 3D patient-specific QA showed that most dose degradation occurred at the edges of the PTV and was not clinically significant. In fact, the largest error that was found did not occur at the isocenter plane and therefore may have been missed by 2D verification techniques. For all the cases that were reconstructed, the leaf positions had a maximum error of -0.26 mm and mean error of 0.15 mm, while the gantry angle deviation was less than  $1^\circ$  and the total MU within 0.5 of the planned values. This method of patient-specific QA is less time consuming than traditional patient-specific QA using detector arrays and electronic portal imaging devices. It also allows for 3D dose reconstruction, and reconstructed plans can be

evaluated in the same software as the original plan. However, the validity of this method is based on the accuracy of the information recorded in the log files, rather than the dose measured directly by a dosimeter array. For instance, the logged leaf positions are taken from the same encoders than position the leaves. There remains some uncertainty in ascribing the reconstructed dose to the actual dose delivered to the patient, as this method assumes that the machine gantry angle, dose rate, leaf position, and output that are recorded in log files are faithful to the machine delivery itself[21].

An alternative approach to VMAT patient-specific QA was initially presented by Létourneau et al.[22]. A hollow cylindrical phantom, embedded with 124 diodes spaced 2 cm apart in the walls to form four rings of detectors, was evaluated. The ability to measure composite dose, reproducibility, and angular dependence of the diodes were measured, and a correction factor was generated for each diode as a function of gantry angle based on the ratio of individual diode response and the mean diode response curve. Up to 4% gantry angle dependent sensitivity was observed. After calibration of the diode sensitivity as a function of irradiation angle there remained a residual angular dependence. VMAT QA was assessed by delivering three VMAT plans to the phantom. The relative dose measured with the dosimeter was compared to the treatment planning system dose distribution. Results indicated that greater than 86.4% of diodes satisfied a 3% relative dose difference and 2 mm DTA for plans with 180 control points[22]. Gantry angle scaling and offset errors were intentionally introduced as well to test the sensitivity of the dosimeter to VMAT delivery errors, with the dosimeter able to resolve a  $1^\circ$  gantry offset error with a reduction in passing rate of  $\geq 9\%$  for 3% and 2 mm tolerance while reduction in the arc length by 0.8% showed pass rate reduction varied between 6.4% and 12.1%. The dosimeter tested by Létourneau offers real-time read-out and invariant perpendicular incidence on the beam central axis for any gantry angle, being able to measure the

beam both on entrance to and exit from the phantom. While diodes have a high sensitivity, the spatial resolution of this device is limited by the small number of diodes covering the available surface space.

Another effort at patient-specific QA by Korreman et al.[23] used a cylindrical PMMA phantom with two crossing orthogonal planes embedded with 1069 p-Si diodes. An inclinometer provided independent information about gantry angle during delivery. Nine treatment plans were delivered to the phantom and the dose distributions were compared to the calculated doses from the treatment planning system. The treatment plans consisted of five prostate plans and four head-and-neck plans. Plans re-delivered on the same day, as well as plans re-delivered on consecutive days, showed good agreement, with gamma values of all points below 1 for a criteria of 3% dose difference relative to the maximum dose delivered and 3 mm DTA. Sub-arc reproducibility indicated that there were large deviations on the control point level, although no deviations in the total accumulated dose were observed. When planned and delivered doses were compared for the patient test-cases, the fraction of passed gamma values was above 95% for all measurements. Like the cylindrical phantom discussed previously, this phantom also has the convenience of a cylindrical shape. However, creation of the 3D dose distribution requires accurate interpolation between the two measurement planes, leading to another source of uncertainty[23].

Bush[24] investigated the use of Monte Carlo (MC) simulation to verify treatment planning calculations by constructing the Monte Carlo beam and patient models from the planned DICOM dataset. MC simulation dose distributions were compared to the dose distributions calculated by the treatment planning system, which were based on an anisotropic analytical algorithm (AAA). While this method did show better than 1% agreement of the dose at isocenter between MC and the original plan, and a maximum dose difference of -0.8%, there are inherent limits to using a MC simulation. This MC model takes into account many complex components

of delivery by explicitly modeling dynamic MLC motion, tongue and groove effects, as well as interleaf leakage, and it allows for modeling of options that are not yet clinically available, such as simultaneous motion of all movable parts of the delivery unit, including collimator, jaws, and couch. However, because the model is based on the 177 control points of the plan DICOM, the gantry and MLC movement between control points must be simulated based on averaging and interpolation. This results in MLC leaf speeds between adjacent control points which are constant, although speed may vary on a per-leaf basis. And, while the model shows good agreement with the treatment planning system, the time for computation is 59.5 minutes. This amount of time provides no additional efficiency to patient-specific QA, and as it provides no direct dosimetric measurement, the benefit of almost full automation of QA appears to come with some inconveniences.

An attempt to combine MC and direct dose measurements has been made by Ceberg et al.[25] using a 3D gel measurements for VMAT verification. 3D gel dosimetry has the advantage of measuring the absorbed dose to an entire volume as well as a response that is gantry angle independent and provides a high resolution. The authors recommend the gel measurement as an additional safety check to quality assurance procedures that are not fully controlled by conventional IMRT techniques. The gel dose matrix was normalized to 100% of the expected dose using the mean value in a  $10 \text{ mm}^3$  volume close to the isocenter in a region of homogenous absorbed dose. A 3D gamma evaluation showed good agreement between both the gel and MC measurements with the treatment planning system planned dose distribution. More than 95% of the the treatment planning system points were within a 3%/3mm passing criteria for both gel and MC. Despite the high pass rate, 3D gels necessitate a great deal of manual effort. The gel described by Ceberg et al. requires manual preparation 24 hours in advance of use, and must be stored in a dark location. An MR scan is needed to read-out each gel dose matrix, but reproducibility between different

sets of gels was found to be high. Additionally, a CT scan of the gel can result in changes to the gel material due to the absorbed dose, although the authors believe that this change is negligible compared to the dose delivered by the planned treatment itself. Temperature gradients must be considered during imaging, so the gel must be given time to reach the equilibrium temperature of the room in which it will be imaged, either by the CT or the MRI machine. The wall of the container which holds the gel can result in MR artifacts or inhomogeneities in the gel itself up to 10 mm into the phantom, while absorbed dose has a standard uncertainty of 3% after background subtraction. Efforts by Sakhalkar et al.[26] have made progress in addressing temporal stability of response (stable more than 90 hours post-irradiation) of a novel gel with an optical-CT readout. The use of optical-CT provides a more easily available and cost-effective option than an MR scanner. The gel presented by Sakhalkar et al. demonstrates a highly linear response to dose, and both robustness and reproducibility of response, with a 94% pass rate with a gamma criteria of 4% dose difference and 3 mm DTA when compared to the treatment planning system calculated distribution. Both noise and edge artifacts remain (scans taken to within 4 mm of the edge), but efforts to reduce both are being investigated[26].

Mans et al.[27] utilized an electronic portal imaging device (EPID), with a 2.5 mm thick copper plate providing build-up, for dose verification both pre-treatment and in-vivo by using in-house developed software. The software was able to separate EPID measurements into frames (2.5 frames/s) while also modifying the measured data with calculations to account for the effect of the inverse square law, attenuation of the beam due to phantom or patient transmission, the effect of the couch on transmission, scattered radiation from various sources, compensation for detector flex as a function of gantry angle, change in detector sensitivity between calibration and measurement dates, and 3D dose reconstruction. Mans et al. reports that implementation of the EPID's read-out mechanism can result in artifacts at beam-

off, beam-on, and changes between discrete dose-rate levels, although these effects are averaged out in the accumulated image. EPID movement, either in the detector plane as allowed by the support arm in order to acquire off-axis images, or in ‘flex’ which is the displacement due to gravity and is angle dependent, must also be accounted for by manually aligning a subset of EPID frames with the treatment planning system control point distributions and using the manual shifts to automatically align the remaining images. Creating a 3D dose distribution requires back projection of the frames and application of couch transmission data to each individual frame, while the EPID sensitivity correction is applied to the total 3D dose. Although the back projection method used did not include an inhomogeneity correction, Mans et al. reports good results for verification using EPID measurements. For pre-treatment verification, the dose was delivered to a phantom for four patient plans and a 3D gamma analysis (3% maximum dose, 3 mm DTA) with an average percentage of points with  $\gamma \leq 1$  of 99%. In-vivo verification of two plans showed similarly high results, with the lowest passing rate having 93% of points in agreement. For a head-and-neck case, the isocenter dose difference was fairly large (-4.7%), but the investigators speculate that this was due to a dose gradient located at the isocenter. EPID’s have the advantage of high resolution when compared to other QA devices, but they have the disadvantage of being highly non-tissue equivalent. EPIDs measure the dose response of the imager rather than the dose to a tissue equivalent phantom, and as Mans et al. acknowledges, there are many modifications that must be made to the measured data before it can be compared to the treatment planning system dose distributions. As well, the weakness of the algorithm used here to include inhomogeneity limits the range of clinical sites which could be verified, while the inability of the technique to distinguish errors in gantry angle limit the usefulness as a QA device.

## 2.5 MatriXX Evolution

The MatriXX<sup>Evolution</sup> is a verification phantom provided by IBA dosimetry (Bartlett, TN). The MatriXX<sup>Evolution</sup> system consists of a 2D ionization chamber array (referred to as the MatriXX) capable of readout resolution of 20 msec. 1020 vented ion chambers are arrayed on a  $32 \times 32$  grid which provides an active area that is  $24.4 \times 24.4$  cm<sup>2</sup>. The center-to-center distance between ion chambers is 7.619 mm. The outer dimensions of the phantom are  $560(l) \times 60(h) \times 320(w)$  mm. Each ion chamber is  $4.5 \times 5(h)$  mm with a chamber volume of 0.08 cm<sup>3</sup>. When irradiated, the air in the chambers is ionized. Charge released by the ionization is separated by an electric field applied between the bottom and top of the electrodes. The bias voltage is  $500 \pm 30V$ . The current is measured and digitalized by a non-multiplexed 1020 channels current sensitive analog to digital converter (ADC). The ion chamber response is transmitted to a PC via a standard Ethernet cable[28]. The typical sensitivity of the ion chamber is 0.42 Gy/nC.

Included in the MatriXX<sup>Evolution</sup> system is a gantry angle sensor which is affixed to the gantry during measurement. The accuracy of the angle sensor is  $\pm 0.5^\circ$ . Build-up and backscatter material is provided in the form of the MULTICube, which allows the MatriXX to be positioned at a given depth, as well as in coronal and sagittal positions on the couch. The MULTICube is made from Plastic Water<sup>®</sup>, which provides dose measurements with an accuracy within 0.5% of the true water dose for energies from 150 keV to 100 MeV. The MULTICube dimensions are 31 cm  $\times$  34 cm  $\times$  22 cm.

The MatriXX<sup>Evolution</sup> is calibrated so that it can provide a measurement of absolute dose in each ion chamber ( $D_{i,j}$ ). The manufacturer supplies a calibration of the gain for individual ion chambers and the user determines the absolute calibration of the detector response. The conversion from charge collected by the MatriXX<sup>Evolution</sup>'s

internal electrometer to absolute dose in the detector plane is described by equation 2.3

$$D_{i,j} = (M - B) N_{DW}^{60Co} K_{i,j}^{uni} K_{i,j}^{off} K^{T,P} K^{user} \quad (2.3)$$

where  $M$  is the raw measured reading,  $B$  is the background reading,  $N_{DW}^{60Co}$  is the calibration factor,  $K_{i,j}^{uni}$  is the uniformity correction at location  $(i, j)$  which is provided by the production site,  $K_{i,j}^{off}$  is the off-axis calibration factor,  $K^{T,P}$  is the temperature and pressure correction, and  $K^{user}$  is the user calibration factor for the detector. In order to determine  $K^{user}$ , the MatriXX<sup>Evolution</sup> is irradiated while in the MULTICube with a  $10 \times 10$  cm AP field[29], providing a known dose at the depth of the ion chamber.

OmniPro-I'mRT software (v. 1.7, IBA Dosimetry, Bartlett, TN) facilitates comparison of MatriXX measurements and treatment planning system imports using visual comparison or mathematical analysis. Measurements with the MatriXX<sup>Evolution</sup> can be displayed as individual frames as well as composite dose distributions. The angular dependency of the ion chambers is optimized by a gantry angle dependent correction factor which utilizes the gantry angle measurement from the gantry angle sensor.

Two sets of correction factors are provided by the manufacturer. The first of these has been created from delivery of a set of static fields with incident angles between  $0^\circ$  and  $180^\circ$  with an angular resolution of  $5^\circ$  except between gantry angle  $85^\circ$  and  $95^\circ$  where an angular resolution of  $1^\circ$  was used. The OmniPro I'mRT software assumes symmetry between the angles which range from  $0^\circ - 180^\circ$  and  $180^\circ - 360^\circ$ , which results in mirroring of correction factors where, for example, the correction factor for gantry angle  $90^\circ$  is used for gantry angle  $270^\circ$ . This set of correction factors will be referred to as 180CF[30].

The second set of correction factors were created in an identical method but without assuming symmetry between gantry angles  $0^\circ - 180^\circ$  and  $180^\circ - 360^\circ$ . Correction factors were determined by the delivery of static fields with incident angles between  $0^\circ$  and  $360^\circ$  with an angular resolution of  $5^\circ$  except between gantry angle  $85^\circ$  and  $95^\circ$  as well as  $265^\circ$  and  $275^\circ$  where an angular resolution of  $1^\circ$  was used. This set of correction factors will be referred to as 360CF.

Neither set of correction factors provided by the manufacturer is ion chamber specific, as a single value is used to correct every individual ion chamber at a given gantry angle. This value is based on the averaged result from the four central ion chambers.

Both sets of correction factors are stored in “comma separated value” (.csv) files which, in addition, contain the linear accelerator name, nominal beam energy, and  $TPR_{20/10}$ , also known as the beam quality index (BQI). These files are provided by the manufacturer for energies of 6 MV and 18 MV with BQIs of 0.666 and 0.783 respectively. These BQI values are assumed to be representative of beams of these energies. When the correction factors are applied to data measured with the MatrixX, it is possible to select the BQI and energy for each unique linear accelerator. The BQI determined for the user created 6 MV and 15 MV correction factors are 0.6767 and 0.7598 respectively. The software linearly interpolates between the default BQI and the custom BQI to create a customized correction factor for the measured data[30].

The BQI is determined by the tissue phantom ratio  $TPR_{20/10}$ , which is calculated as shown in equation 2.4

$$TPR_{20/10} = 1.2661 \times PDD_{20/10} - 0.0595 \quad (2.4)$$

where  $PDD_{20/10}$  is the ratio of the percent depth dose at 20 cm and 10 cm depths for

a field size of  $10 \times 10 \text{ cm}^2$  defined at the phantom's surface with a source-to-surface distance of 100 cm.

### *2.5.1 Clinical Verification of the MatriXX*

With the MatriXX in a gantry holder, dosimetric evaluation has been carried out by Herzen et al.[31]. Dose and energy dependence, response during initial warm-up, and stability over time were examined. The number of MU's was varied between 10 – 1000 MU for 4 MV, 6 MV, and 15 MV energies for a  $10 \times 10 \text{ cm}^2$  field and a source-to-effective-point-of-measurement distance of 100 cm with 5 cm solid water build-up. The dose for each energy was determined using an independent dosimeter. A linear correlation between dose and signal was found for all energies as a result of the average signal of the four central pixels. The signal from the MatriXX increased linearly with dose and the signal was not found to depend on beam energy for the range of 4 MV to 15 MV x-rays. Repeated irradiation during a warm-up period of 30 minutes indicates that the MatriXX must be pre-irradiated before starting a measurement and after a break if the device is turned off in order to achieve reproducible results. The spatial response of a single ion chamber was examined using a line spread function determined from data measured from a narrow shifted slit of irradiation across the chamber. Results indicate that the dose measured in cross-plane and diagonal directions can be treated as isotropic. In order to compare the measured absolute dose distribution and the calculated dose distribution, the detector was calibrated[32] to achieve a homogeneous response and calibrated per manufacturer's instructions. The MatriXX was irradiated with the gantry set to zero, and good agreement was found between calculated and measured response. The maximum deviation of the corrected measured line profile was 8.4% in the region of large gradients, although this was as high as 16% in the un-corrected profile[31].

### *2.5.2 Evaluation of the MatriXX Device in Patient-Specific IMRT Verification.*

Evaluation of the MatriXX for step-and-shoot IMRT was carried out by Cheong et al.[33]. A 6 MV x-ray treatment plan was delivered with seven field step-and-shoot IMRT delivery for a lung treatment. The MatriXX was evaluated for consistency, reproducibility, and accuracy. The MatriXX was positioned between 10 and 4.7 cm solid water slabs of backup and build-up material respectively. A Farmer-type ion chamber was used to validate the MatriXX reading of absolute dose, and dose rates of 1-100 MU were delivered to a  $10 \times 10$  cm<sup>2</sup> field for both Farmer chamber and MatriXX. The average dose in a  $4 \times 4$  cm<sup>2</sup> area was compared to the Farmer chamber point dose reading. Results indicated that both the MatriXX and ion chamber underestimated doses delivered with low dose rates and small MU's while overestimating delivered MU in the case of high dose rates. However, this discrepancy was less than  $\pm 1\%$  for MU's greater than 3. As well, 100, 300, and 600 MU were delivered at a dose rate of 100, 300, and 600 MU/min respectively and the average dose in the  $4 \times 4$  cm<sup>2</sup> area was determined. This consistency test indicated that at a 100 MU/min dose rate there was the possibility that the MatriXX may fail to capture all signals during a discrete sampling time, with a frame to frame variance ( $3\sigma$ ) of 12.2%. However, as dose rate increased, the frame-to-frame variance decreased, while the integral dose per monitor unit remained constant for all dose rates. Reproducibility was determined by delivering an IMRT field ten times at different dose rates, comparing planned and delivered MU, and based on the mean and standard deviation of the data the reproducibility of the MatriXX was found to be good[33].

The MatriXX has also been used in VMAT patient-specific verification as described by Boggula et al.[34]. The COMPASS<sup>®</sup> system allows for 3D dosimetric quality assurance using MatriXX-specific software and the MatriXX mounted to the gantry with a gantry angle sensor. VMAT patient plans were delivered to the

MatriXX and used to verify the 3D dose distribution calculated by COMPASS. A systematic deviation was noticed in the measurement-based dose reconstruction provided by COMPASS which resulted in overestimation of the dose by nearly 2% in the ion chambers. This overestimation was attributed to large open fields creating excessive electron contamination and it was believed that the commissioning of the COMPASS beam model was not optimal for large field sizes. Detector resolution could also contribute to large deviation between calculated and measured results for highly modulated fields. As well, low dose rates ( $< 5\text{MU}/\text{min}$ ) were sometimes recorded as having no response for a few frames[34].

### *2.5.3 Investigation of Angular Dependent Response*

The MatriXX has been investigated for VMAT patient-specific verification while positioned on the treatment couch rather than in the gantry holder [35, 36, 37, 29]. This couch-based setup allows for the cumulative planned dose in a single plane to be measured. However, the angular dependence of the MatriXX is not fully accounted for by the calibration utilized by OmniPro software [30] which relies on the components of equation 2.3.

The inherent angular dependency of the MatriXX<sup>Evolution</sup> has been investigated by Wolfsberger et al.[29] for an absolute calibration dependent on an AP field. It was concluded that the angular response of the MatriXX is independent of attenuation from the phantom used and cannot be accounted for by the uncertainties in the density of the materials inside the MatriXX or by the uncertainty in Hounsfield units (HU) in the planning CT. The doses measured by the MatriXX device within build-up and backscatter material (MatriXX phantom) were compared to those calculated in a uniform phantom without the MatriXX device (reference phantom), with all other geometry closely matching that of the MatriXX phantom for optimal results. Dose to the reference phantom was measured independently with an A12 ionization chamber

placed along the axis of gantry rotation. Measurements were acquired within a  $30 \times 30 \text{ cm}^2$  solid water slab for 6 MV beams of  $10 \times 10 \text{ cm}^2$  field size irradiated every  $10^\circ$  except for angles  $90^\circ - 110^\circ$  and  $270^\circ - 260^\circ$  which were irradiated in  $1^\circ$  increments. A calibration factor was established using the dose measured by the MatriXX,  $D_{measured}(\theta)$ , and the dose calculated,  $D_{ref}(\theta)$ , at each angle

$$CF(\theta) = \frac{D_{measured}(\theta)}{D_{ref}(\theta)} \quad (2.5)$$

Wolfsberger et al. uses this calibration factor to correct measured dose,  $D_{QA}$ , to calibrated measured dose,  $D_{QA}^{calib}$ , as shown in equation 2.6

$$D_{QA}^{calib}(\theta) = \frac{D_{QA}(\theta)}{CF(\theta)} \quad (2.6)$$

In-house software was used to take individual “snaps” from the MatriXX record of dose per time and apply the calibration factor based on the angle of the recorded snap. The corrected dose distributions were summed for comparison with the cumulative dose from the treatment planning system, with VMAT plans having two full arcs for each plan ( $179^\circ \rightarrow 181^\circ$  and  $181^\circ \rightarrow 179^\circ$ ). Wolfsberger et al. also verified that water equivalent build-up and scatter of the MatriXX met manufacturer specification, investigated the contribution of high-Z material within the MatriXX to AP/PA discrepancies in dose, and also considered the off-axis dependence for open beams which was compared to dose profiles collected in a water tank with a small-volume ion chamber. The MatriXX angular and attenuation dependence for one of four detectors indicated that the ratio of AP to PA dose ranged between 7% to 11% with good reproducibility of response from 0.5% to 1%. Absolute dose for AP fields was found to be within 1% of the user calibration. Wolfsberger et al. found that patient-specific QA without angular dependency correction showed a similar dose distribution shape when compared to the treatment planning system

calculated dose but magnitudes of measured dose which were consistently smaller. Using the calibration factor improved the agreement. Additionally, plans with higher dose gradients demonstrated a larger deviation between the MatriXX measured dose and the independent ion chamber measurement. A dose bias of approximately  $-3\%$  was observed when dose was not corrected for by the calibration factor. The high-Z material was found to be properly accounted for in the planning system for all angles, and the calibration factor was found to be shift-invariant based on the agreement of off-axis ion chamber response to a reference ion chamber in water for a  $10 \times 10 \text{ cm}^2$  field. Rescaling MatriXX doses by the calibration factor lead to agreement to within  $\pm 0.7\%$  of readings for MatriXX ion chambers with larger discrepancies at the edges of the field[29].

The inherent angular dependence was determined to not entirely be due to uncertainties in water equivalent thickness. Wolfsberger et al. postulated that another effect occurring at the air-to-high-Z material interface for the PA beams was likely responsible for AP/PA discrepancies in dose, which cannot be accurately accounted for within the treatment planning system. For lateral beams, the cause of the angular dependence was attributed to effective path length and resulted in a sharp dose drop. Additionally, high sensitivity to misalignment was found for gantry angles between  $91^\circ - 110^\circ$  and  $260^\circ - 269^\circ$ , although they were not found to greatly bias the overall VMAT QA. Overall, the calibration method reduced bias from  $8\% - 11\%$  for PA fields to  $\approx 1\%$ [29].

Hybrid plan verification of IMRT fields using the MatriXX has also been investigated by Dobler et al.[36]. Using open fields with gantry angles in steps of  $10^\circ$  increments, the dose was calculated on a CT scan of the MatriXX. Slabs of RW3 (PTW, Freiburg, Germany) were used as build-up and backscatter material. An ion chamber was positioned at the level of the MatriXX ion chamber array above the couch, and irradiated for a reference field of  $10.4 \times 9.6 \text{ cm}^2$  field size for 36 evenly

spaced gantry angles at 100 MU. The attenuation  $A$  was determined using equation 2.7.

$$A = \frac{dose(x^\circ)}{dose(0^\circ)} - 1 \quad (2.7)$$

The number of monitor units was reduced in the treatment planning system calculation of the phantom plan with respect to the couch attenuation for the respective gantry angle. The plans were irradiated onto the phantom with the original number of monitor units. Attenuation of up to 7% could be observed for the iBeam<sup>®</sup> couch top, although only a slight improvement was noted when couch attenuation was taken into effect. Verification of single beam plans indicated that measured dose was in general higher than calculated for gantry angles 0° – 70° and lower for 100° – 180°, although the study did not investigate angular dependence further. Seventeen IMRT plans were transferred to a CT study of the MatriXX and recalculated using pencil beam, collapsed cone, and Monte Carlo algorithms. The results of this study indicate that hybrid plan verification, in which the original gantry angles are retained for the phantom plan, passed the gamma test (> 95% pixels) with 4% dose tolerance and 3 mm DTA in all seventeen IMRT cases. It was determined that the MatriXX is best suited for hybrid plan verification criteria of 3% and 3 mm if a relaxed dose tolerance of 4% is used in low dose regions outside the MLC, but it is unclear if these results were determined with absolute or relative MatriXX measurements.

Other methods have been utilized to correct for the angular dependency of the MatriXX. The University of Alabama at Birmingham[35] was the first site to use RapidArc clinically in the United States, and used the MatriXX together with film and single ion chamber measurements for patient-specific QA. The MatriXX was oriented coronally on the treatment couch within the MULTICube. A C-shaped contour was created below the MatriXX in verification QA, with a CT number adjusted for best match based on central axis measurements from various angles using a 10 × 10

cm<sup>2</sup> field. Couch attenuation was modeled in Eclipse, so the C-shaped contour is intended to account for the inherent angular dependence as described by Wolfsberger et al.[29], although further investigation into the cause of the angular dependence is not described. The isocenter of the hybrid verification plan was adjusted such that the single ion chamber would lie in a high dose, low gradient region and the MatriXX array center was adjusted to lie at the same position as the single ion chamber used for film normalization. The comparison of film and MatriXX results indicate fewer regions of failure ( $\gamma < 1$ ) were found when using the MatriXX, where the reference dose used was the average dose to the four central ion chambers as calculated by the treatment planning system.

In order to compare plan quality, delivery efficiency, and accuracy of VMAT and helical tomotherapy (HT) plans, Rao et al. [37] used the MatriXX ion chamber array within the MULTICube phantom for VMAT plan verification. The dose distribution for each plan was re-calculated to the CT scan of the phantom. Angular dependence was attributed to couch attenuation in the posterior direction and a 1.2 cm thick water equivalent contour was added under the phantom in each VMAT QA plan. Using this method, the MatriXX verification measurements of 18 VMAT plans, including prostate, head-and-neck, and lung cases, showed the absolute dose measurement to be in good agreement with calculated values, having an average passing rate of 98.7% for gamma analysis of 3 mm DTA and 3% absolute dose difference[37].

## 2.6 Aims

The need to verify the accuracy of dose delivery has never been greater than with VMAT. However, no single measurement technique or device has become widely accepted for VMAT patient-specific QA. An attempt to develop an accurate and reproducible QA protocol with the MatriXX<sup>Evolution</sup> will be investigated here.

The examination of the MatriXX<sup>Evolution</sup> involves the construction of an ion

chamber-specific correction factor, providing a unique correction for the angular dependence of individual ion chambers over a full 360°. The correction factors generated by the user will be produced for specific photon energies, including both 6 MV and 15 MV, the latter of which is not otherwise provided by the manufacturer. Use of the default correction factors would rely on interpolation between a 6 MV and 18 MV photon beam. As well, the user correction factors will be created using two different set-ups of the MatriXX<sup>Evolution</sup> in order to examine the effect of the couch on the MatriXX<sup>Evolution</sup>'s response. Finally, the effect of gantry direction will also be investigated by the comparison of response between counterclockwise and clockwise arc delivery.

## Methods and Materials

### 3.1 Equipment

#### *3.1.1 MatriXX Treatment Planning and Set-up*

The ion chamber array (ICA) consists of 1020 parallel-plate ion chambers placed within phantom material described previously in Section 2.5. CT scans of the ICA were taken in three orientations. The ICA was positioned in both coronal and two distinct sagittal set-ups on the couch with the assistance of laser alignments. In the coronal position, the ICA was positioned such that the detector plane faced gantry angle  $0^\circ$  (coronal orientation) as shown in Figure 3.1. Sagittally, the ICA was positioned with either the detector facing gantry angle  $270^\circ$  (sagittal270 orientation) or facing gantry angle  $90^\circ$  (sagittal90 orientation).

Dose calculation was performed with the Eclipse treatment planning system v.8.6 (Varian Medical Systems Inc., Palo Alto, CA) using the analytical anisotropic algorithm (AAA) with a 2.5 mm grid size. Doses were further interpolated to a 1 mm grid size when exported for comparison with measurements. The RapidArc<sup>®</sup> algorithm (Varian Medical Systems Inc., Palo Alto, CA) was used to design and deliver the VMAT plans.

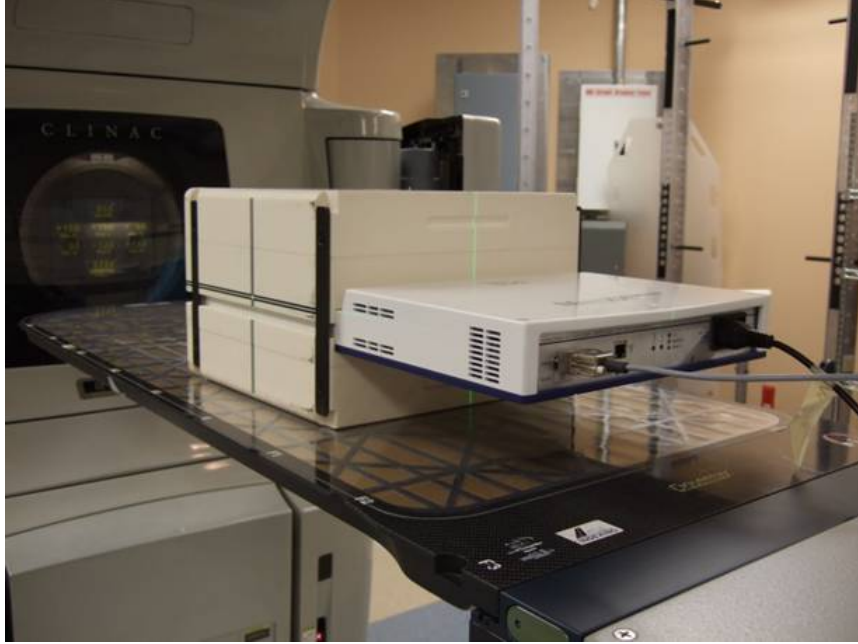


FIGURE 3.1: The ICA is shown positioned on the couch in the coronal position.

### 3.1.2 Measurements

The ICA was connected to a gantry angle sensor, power source, and PC as shown in Figure 3.2. Measurements were evaluated using OmniPro I'mRT v.1.7 software (IBA Dosimetry GmbH, Schwarzenbruck, Germany).

All treatment fields were delivered by a Varian model linear accelerator (Clinac 21EX S.N. 2325 and Novalis S.N. 3691). The Clinac 21EX linear accelerator measurements were taken with a DoseMax couch with movable carbon fiber rails (Q-Fix Systems, Wyckoff, NJ) while the Novalis linear accelerator used a 6D carbon fiber couch without rails (BrainLAB AG, Feldkirchen, Germany).

The gantry angle sensor (GAS) was attached to the gantry and leveled using two attached locking screws. Alignment was indicated by LEDs. The GAS reading when the gantry was at  $0^\circ$  and  $270^\circ$  must agree within the OmniPro software to within  $0.5^\circ$ .

As recommended by the manufacturer[28] and Herzen et al.[31], the ICA requires

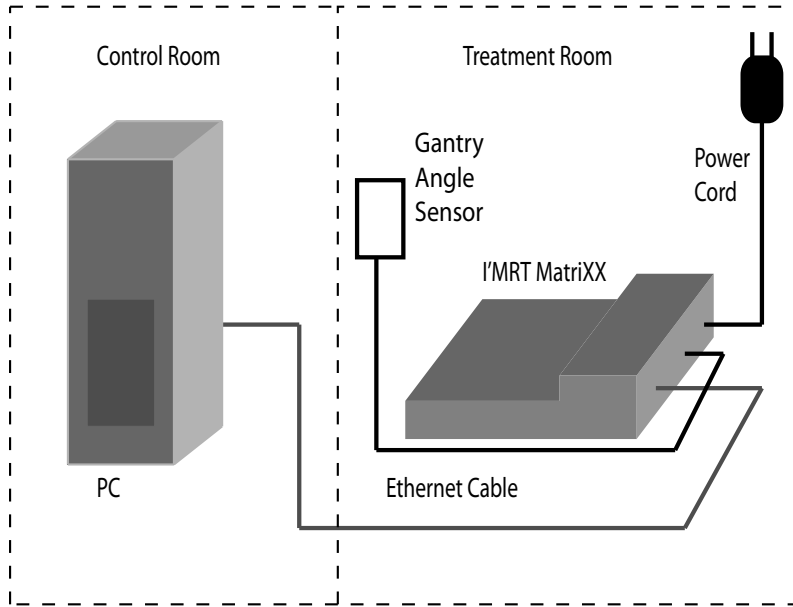


FIGURE 3.2: The diagram shows the general connections between the ICA, the power supply, gantry angle sensor and the PC.

pre-irradiation prior to use in order for the ion chamber signals to reach a stable value. Regardless of set-up orientation, the pre-irradiation open field was delivered en face to the ICA.

The signal from the ICA without any beam incident on it (the background signal) must be collected so that it can be automatically removed from subsequent measurements.

## 3.2 ICA Evaluation

### 3.2.1 Consistency

Consistency of the ICA response was measured by delivering 5 identical open fields ( $32 \times 32 \text{ cm}^2$ ) en face. Both 6 MV and 15 MV energies were used to deliver 200 MU at a dose rate of 400 MU per minute. The resulting five measurements were averaged for each ion chamber. The difference between each measured ion chamber response and the average response was taken for each of the five measurements. The average

and standard deviation was found for this difference for all ion chambers and all 5 measurements.

### 3.3 Intrinsic MatriXX Response

The effect of the high density layer below the plane of the ion chambers was investigated to determine whether the high density layer perturbed the radiation, possibly creating more secondary electrons. This possibility was examined by measuring both clockwise and counterclockwise arc-based deliveries, as it was hypothesized that a stationary gantry delivery would not see any composite effect due to this layer. As well, MLC sliding window fields were delivered en face to the ICA to determine the effect of narrow field sizes which are similar to those used in VMAT treatment plans.

#### *3.3.1 Counterclockwise vs. Clockwise: Open Field Stationary Angles*

While a CW and CCW dependence in the ICA response was only likely to be seen in arc-based delivery, static open fields were also delivered CW and CCW to ensure that any subsequent dependence was indeed unique to arcs. Open fields  $32 \times 32$  cm<sup>2</sup> were delivered CCW and CW at static gantry angles every 30° beginning at gantry angle 180°. For each field, 100 MU was delivered at 600 MU per minute for both 6 MV and 15 MV beams. At each delivery angle, the difference between CCW and CW ion chamber responses was taken, and the average and standard deviation of all ion chambers for all CCW/CW pairs computed.

#### *3.3.2 Counterclockwise vs. Clockwise: Open Field Arcs*

Open field partial arcs were also delivered both CCW and CW for 6 MV and 15 MV beams. A  $32 \times 32$  cm<sup>2</sup> field size was used, with 100 MU delivered every 45° at a dose rate of 400 MU per minute. Five arcs were used in total as shown in Table 3.1, delivered first CCW and then CW. The difference between ion chamber responses for

Table 3.1: Open field partial arcs subtending angles of  $45^\circ$  and  $90^\circ$ , and the respective number of monitor units delivered to achieve  $2.22 \frac{MU}{\circ}$ .

Arcs	MU
$180^\circ - 135^\circ$	100
$135^\circ - 45^\circ$	200
$45^\circ - 315^\circ$	200
$315^\circ - 225^\circ$	200
$225^\circ - 180^\circ$	100

CCW and CW pairs was taken for each arc, and the average and standard deviation of all ion chamber responses for all arcs determined.

### 3.3.3 Counterclockwise vs. Clockwise: Small Field Arcs

To test arc based delivery on field sizes that were on the same order as those used in clinical treatments, 6 MV and 15 MV energies were used to deliver 300-400 MU at 600 MU per minute in a full  $360^\circ$  arc for a  $1 \times 32 \text{ cm}^2$  field defined by the jaws and a  $1 \times 32 \text{ cm}^2$  field defined by the MLC. A  $1 \times 20 \text{ cm}^2$  MLC defined field was used for data collected on the Novalis linear accelerator due to the limits of the HDMLC. For the MLC fields, the jaws were opened to  $12 \times 32(20) \text{ cm}^2$  to evaluate the effect of MLC transmission. The collimator was set to  $0^\circ$  for all fields, which were delivered CCW→CW, and also CW→CCW. The average and standard deviation of the difference between CCW and CW, as well as CW and CCW was determined.

### 3.3.4 MLC Sliding Window Static Gantry

MLC sliding window fields were delivered at gantry angle  $0^\circ$  for 1 mm, 2 mm, 5 mm, and 10 mm gaps at 400 MU per minute for a total of 400 MU using both 6 MV and 15 MV energies.

## 3.4 Creation of Angle Dependent Correction Factors

In order to correct for the inherent gantry angle dependence[29], a  $32 \times 32$  matrix of correction factors was created for the ion chamber readings by taking the ratio of measured dose to calculated dose as described by equation 2.5. Correction factors were created using a subset of gantry angles and both 6 MV and 15 MV beams.

### 3.4.1 Measurement Data

In each orientation (coronal, sagittal270, sagittal90), the ICA was irradiated at static gantry angles with 100 MU delivered at a dose rate of 600 MU per minute and a field size  $32 \times 32$  cm<sup>2</sup>. In the coronal orientation, these measurements were acquired in 5° increments for a full 360° and in 1° increments from gantry angle 85° – 95° and 265° – 275°. In the sagittal orientation, the measurements were acquired from gantry angle 270° – 0° – 90° every 5° and in 1° increments for gantry angles 355 – 5° as shown in Figure 3.3a and Figure 3.3b.

The dose delivered to the ICA was recorded by the OmniPro I’mRT software in “movie mode”, where individual “snaps” are acquired every second during delivery and summed to create an “integral” dose. A full 360° set of correction factors was created by the combination of sagittal270 and sagittal90 measurements as shown in Figure 3.3c. Unlike the correction factors taken with the ICA in the coronal orientation, the sagittal correction factors are not affected by the attenuation of the couch.

### 3.4.2 Eclipse Calculations

Dose distributions were exported from Eclipse in the same plane as the measured readings for each of the orientations described above. The dose distributions were exported in DICOM format, which are compatible with OmniPro I’mRT software. The dose grids were exported in a  $33 \times 33$  matrix. The dose calculated by Eclipse is

used as the gold standard in creating the correction factors.

### 3.4.3 MATLAB

The Eclipse dose distributions which were exported in the form of DICOM images in a  $33 \times 33$  matrix were read into MATLAB<sup>®</sup> and interpolated to a  $32 \times 32$  matrix with dose values located coincident with the center of each ion chamber in the CT scan of the ICA.

Measured dose distributions for each irradiated angle were exported from OmniPro. Within MATLAB, the correction factors were created by dividing the Eclipse calculated dose at each ion chamber (IC) by the ICA measured dose at each ion chamber as shown in equation 3.1. This process was used for both coronal and sagittal orientations of the ICA, at 6 MV and 15 MV energies. See Appendix A for the code used to generate the correction factors.

$$CF(IC, \text{gantry angle}) = \frac{\text{calculated}(IC, \text{gantry angle})}{\text{measured}(IC \text{ gantry angle})} \quad (3.1)$$

### 3.4.4 Statistical Analysis using Paired T-Test

Mirroring of CFs from gantry angles  $0^\circ - 180^\circ$  to CFs from gantry angles  $180^\circ - 360^\circ$  can be statistically analyzed using a paired t-test.

The paired t-test determines whether the two sets differ from each other in any significant way, assuming that the paired differences are independent and identically normally distributed. The test is used to compare two paired sets,  $X_i$  and  $Y_i$  of  $n$  measured values by calculating the difference between each set of pairs, and analyzing the ratio of the mean of these differences to the standard error of the differences. If the ratio is large, the p-value is small, generally indicating that the paired results are considered to be significantly correlated. When using a two-tailed t-test, the p-value represents the probability that, if the null hypothesis (that there is no difference

between the groups) is true, the selected samples would have means as far apart as (or further than) those observed in the two data sets with either group having the larger mean. Using the conventional threshold value for the p-value of 0.05, if the p-value is less than the threshold, the null hypothesis is rejected and the difference is considered to be statistically significant, while if the p-value is greater than the threshold, the null hypothesis cannot be rejected and the difference is not statistically significant.

To apply the paired t-test, let

$$\hat{X}_i = (X_i - \bar{X})$$

and

$$\hat{Y}_i = (Y_i - \bar{Y})$$

where  $\bar{X}$  and  $\bar{Y}$  are the mean values of data sets  $X_i$  and  $Y_i$ , respectively. Defining  $t$ , the test statistic as

$$t = (\hat{X} - \hat{Y}) \sqrt{\frac{n(n-1)}{\sum_{i=1}^n (\hat{X}_i - \hat{Y}_i)^2}}$$

where  $n - 1$  is the number of degrees of freedom. If the p-value associated with  $t$  is low ( $p < 0.05$ ), then there is evidence to reject the null hypothesis.

#### 3.4.5 Smoothing

The ICA holds 1020 ion chambers in a  $32 \times 32$  grid, lacking the four corner ion chambers. A distance weighted interpolation method was used to find the dose at the four corners from the dose at the three nearest ion chambers. The value calculated by the user replaced the value at the corner points which was calculated by the ICA and software. The smoothing of these corners was necessary because

the interpolation method used by the ICA's software created artifacts at the corners that were not representative of the dose to the nearby ion chambers.

## 3.5 Correction Factor Analysis

### *3.5.1 Correction Factor Measurement Consistency*

In order to investigate the consistency of the measurements used to calculate the correction factors, three sets of correction factors were created based on  $27 \times 27$  cm<sup>2</sup> fields delivered on three different days at 6 MV, with the ICA in a coronal set-up. The variability was assessed by measuring the standard deviation of the correction factor for each ion chamber at each gantry angle over all three days, and by finding the average difference between correction factors for each ion chamber.

### *3.5.2 Correction Factor Asymmetry*

The difference between fields delivered for gantry angles  $0^\circ \rightarrow 180^\circ$  and  $180^\circ \rightarrow 360^\circ$  was investigated by finding the mean value and standard deviation of the correction factors at each angle.

## 3.6 CF Verification

The user created correction factors and manufacturer provided default correction factors were compared by taking measurements with the ICA, applying correction factors, and comparing the corrected measurements against the calculated dose exported from the Eclipse treatment planning system using gamma analysis (3% dose difference, 3 mm distance to agreement, 5% threshold). The manufacturer provided two sets of correction factors, 180CF and 360CF, described previously in Section 2.5. This evaluation was carried out for open arc fields and patient plans.

### *3.6.1 Open Arcs*

The correction factor table was validated by its application to  $32 \times 32$  cm<sup>2</sup> open field partial arc measurements with the ICA set-up in the coronal position, using both CW and CCW delivery at 400 MU per minute. The arcs delivered and relevant parameters are given in Table 3.1. The application of both user and default correction factors to the measured ion chamber values was compared for both 6 MV and 15 MV energies.

### *3.6.2 Patient Plans*

Five RapidArc patient plans were delivered to the ICA. Two of the plans used 15 MV arcs created for anal cancer treatments, and three of the plans used 6 MV arcs created for head and neck treatments.

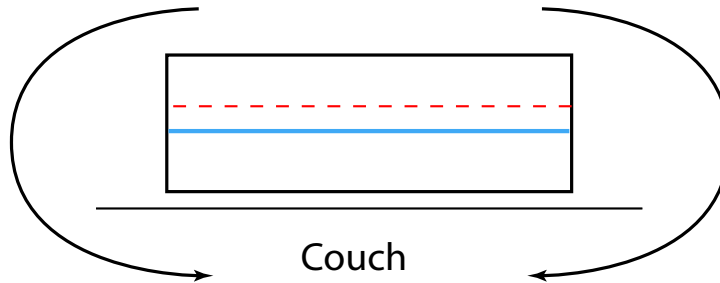
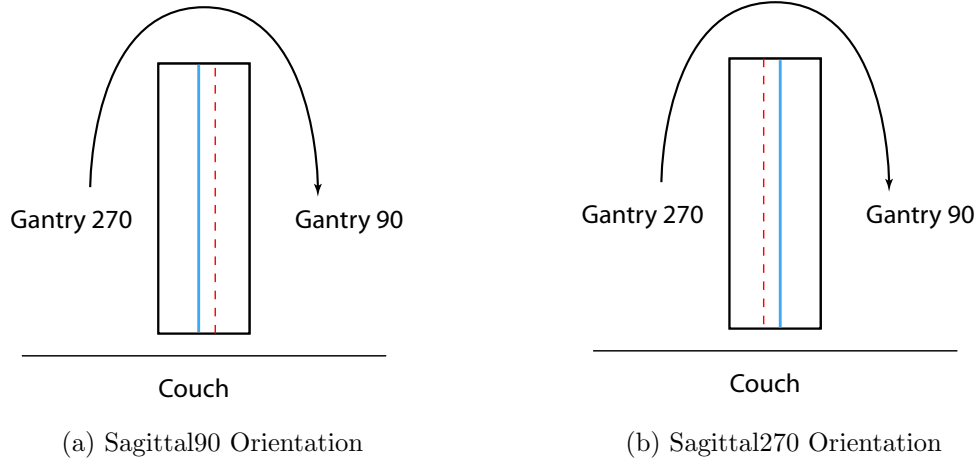


FIGURE 3.3: (a) Sagittal90 Orientation: Measurement includes gantry angles  $270^\circ - 0^\circ - 90^\circ$ . The red dotted line indicates the plane of ion chambers facing gantry angle  $90^\circ$  with the blue line indicating a plane of high density material. (b) Sagittal270 Orientation: Measurement includes gantry angles  $270^\circ - 0^\circ - 90^\circ$ . The red dotted line indicates the plane of ion chambers facing gantry angle  $270^\circ$  with the blue line indicating a plane of high density material. (c) Using the combination of two sagittal measurements creates a new  $360^\circ$  measurement without the effect of couch attenuation. Alternatively, a  $360^\circ$  measurement can also be created with the ICA in the coronal orientation and which does include the effect of the couch in measurements.

# 4

## Results

### 4.1 ICA Consistency

To check the consistency of the results, we calculated the average and standard deviation of each ion chamber's measurement for a set of 5 repeated irradiations. The 6 MV and 15 MV energies both showed an average variation of  $0.0 \pm 0.1$  cGy.

### 4.2 Intrinsic MatriXX Response

#### *4.2.1 Counterclockwise vs. Clockwise: Open Field Stationary Angles*

The static open field arcs which were delivered CW and CCW were analyzed by finding the average difference and standard deviation between the CW and CCW delivery for each ion chamber. For the 6 MV energy, the average difference between repeated fields was  $0.0 \pm 0.0$  cGy. For the 15 MV energy, the average difference between repeated fields was  $0.0 \pm 0.1$  cGy.

#### *4.2.2 Counterclockwise vs. Clockwise: Open Field Arcs*

A similar analysis of CW vs. CCW partial arcs resulted in an average difference between 6 MV arcs of  $-0.1 \pm 0.2$  cGy, and an average difference between 15 MV arcs

of  $0.0 \pm 0.1$  cGy.

#### *4.2.3 Counterclockwise vs. Clockwise: Small Field Arcs*

Analysis of CCW and CW small field measurements are given in Table 4.1. The dose measured by the ICA in the penumbra region (50% of the maximum dose) of each field were analyzed. The results were divided into “left” (patient left for a head-first prone setup) and “right” and analyzed by expressing as a percentage the ratio of average dose to maximum measured dose. The arcs were delivered counterclockwise followed by clockwise, as well as clockwise followed by counterclockwise. No delivery order dependency was observed.

A difference map of 1 cm MLC fields delivered CW and CCW is given in Figures 4.1-4.2.

#### *4.2.4 MLC Sliding Window Static Gantry*

The results of delivering various size MLC sliding window fields with energies of 6 MV and 15 MV are shown in Table 4.2, evaluated by the percent of pixels passing a gamma criteria of 3%/3mm.

### 4.3 Correction Factor Analysis

#### *4.3.1 Correction Factor Measurement Consistency*

The variation of the ion chamber response to the same measurement on different days provides a baseline for correction factor variability. The consistency of the ICA response at various angles was acquired using data collected on three different days, using the set-up described previously in Section 3.4.1 but with a  $27 \times 27$  cm<sup>2</sup> field size. The standard deviation between individual ion chamber responses over those three data sets, averaged for all ion chambers and gantry angles, was 0.0072 Gy. The maximum standard deviation in ICA response was 0.0342 Gy. The average difference

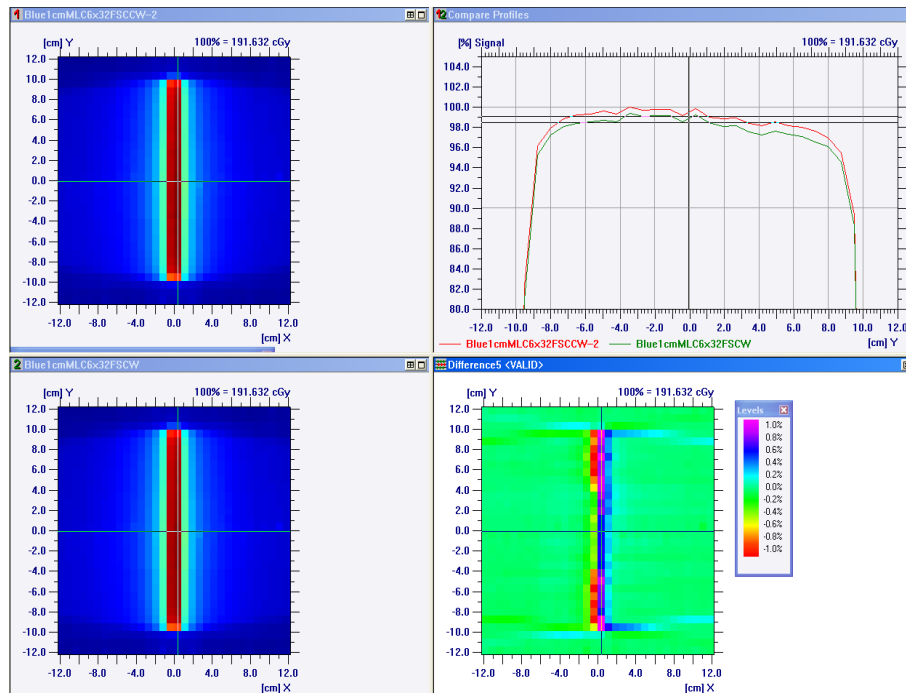


FIGURE 4.1: 6 MV CCW-CW difference map.

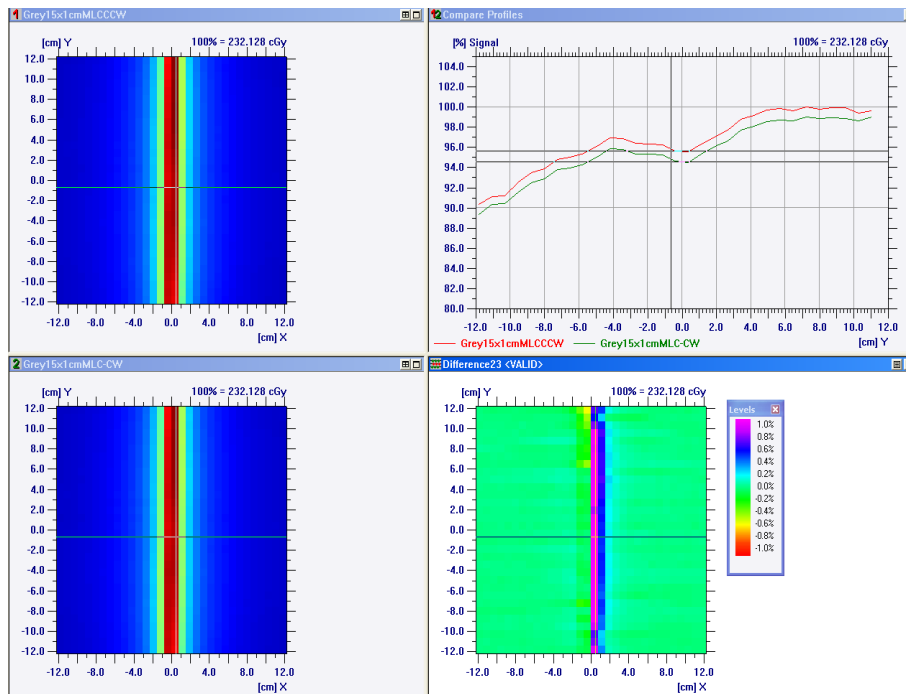


FIGURE 4.2: 15 MV CCW-CW difference map.

between correction factors was  $0.0 \pm 0.0$ .

#### 4.3.2 Correction Factor Asymmetry

Variations in the ion chamber-specific correction factor were observed at each gantry angle. The average correction factors plotted with the standard deviations are shown in Figures 4.3-4.6. The data reported in Figures 4.5 and 4.6 were created using the sagittal90 and sagittal270 orientations of the ICA, but the gantry angles referred to on the x-axis of the plots correspond to a coronal orientation of the ICA (see Figure 3.3).

The 6 MV and 15 MV coronal correction factors, which include the effect of the couch, have a mean value and standard deviation across all ion chambers and gantry angles of  $1.005 \pm 0.023$  and  $1.003 \pm 0.016$  respectively. The 6 MV and 15 MV sagittal correction factors, which are unaffected by the presence of the couch and appear to show slightly reduced ion chamber variation, have a mean value and standard deviation across all ion chambers and gantry angles of  $1.012 \pm 0.018$  and  $1.005 \pm 0.013$  respectively. A maximum standard deviation of 0.046 for the 6 MV coronal correction factor is found at gantry angle  $89^\circ$ . A maximum standard deviation of 0.032 for the 15 MV coronal correction factor is found at gantry angle  $271^\circ$ . The maximum standard deviation for the 6 MV and 15 MV sagittal correction factors occur at the same angles as those of the coronal correction factors, with values of 0.043 and 0.030 respectively. The gantry angles at which large standard deviation values occur ( $\sigma > 0.03$ ) are given in Table 4.3 for both orientations and energies.

Asymmetry in correction factors measured from gantry angles  $0^\circ \rightarrow 180^\circ$  and  $180^\circ \rightarrow 360^\circ$  is shown in Figures 4.7-4.10, where the mirrored averages and standard deviations are plotted on the same x-axis, from  $0^\circ - 180^\circ$ .

Using a paired t-test, the p-values for the mirrored data for 6 MV and 15 MV coronal and sagittal mirrored data sets were all found to have a value of  $p < 0.0001$ ,

Table 4.1: The average and standard deviation of the left and right side ion chamber measurements given as a percentage of the maximum value of both sides for 6 MV and 15 MV small fields.

Small Field Results			
		Left	Right
6 MV	1 cm jaw	$0.0 \pm 0.0\%$	$0.3 \pm 0.2\%$
	1 cm MLC	$-0.4 \pm 0.3\%$	$0.3 \pm 0.3\%$
15 MV	1 cm jaw	$0.1 \pm 0.1\%$	$0.4 \pm 0.2\%$
	1 cm MLC	$-0.2 \pm 0.2\%$	$0.6 \pm 0.3\%$

Table 4.2: The results for 6 MV and 15 MV MLC sliding window static fields are given as the percent of pixels passing a gamma analysis.

MLC Sliding Window Gamma Analysis					
	1 mm	2 mm	3 mm	5 mm	10 mm
6 MV	23.23	21.23	23.31	23.92	46.11
15 MV	48.49	51.52	52.44	55.24	65.1

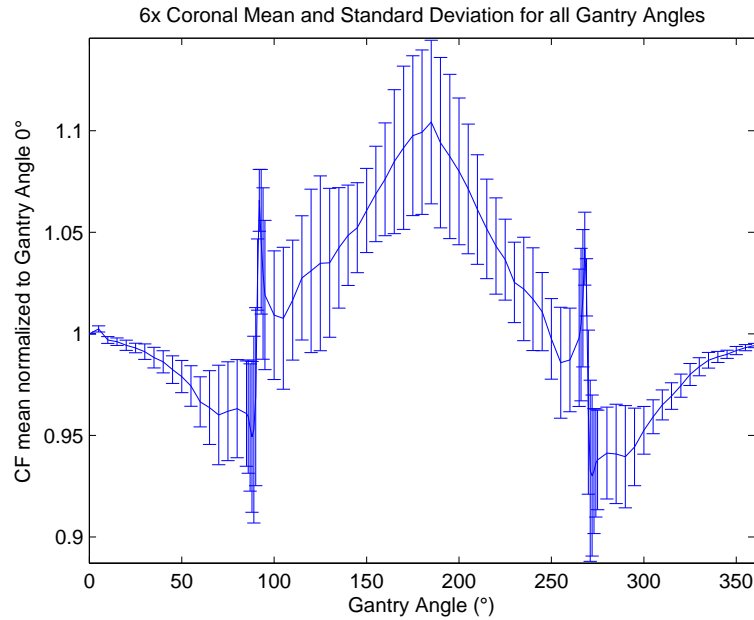


FIGURE 4.3: 6x coronal CF mean and standard deviation.

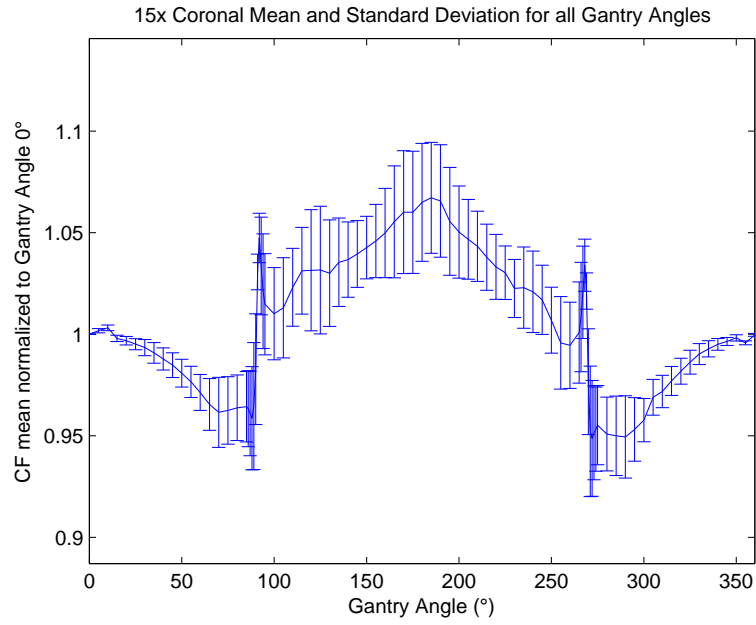


FIGURE 4.4: 15x coronal CF mean and standard deviation.

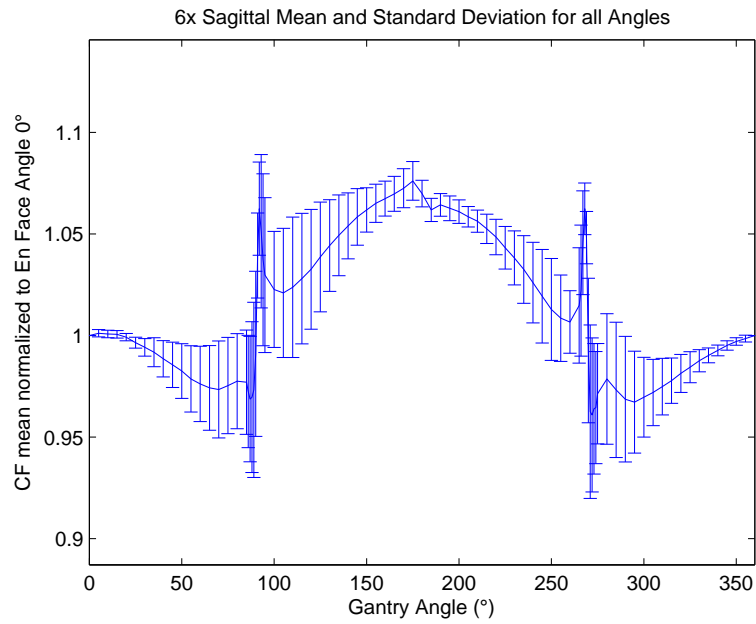


FIGURE 4.5: 6x sagittal CF mean and standard deviation.

indicating that the difference between mirrored data sets can be considered extremely statistically significant. The mean difference in the 6 MV correction factor was 0.012 for the coronal orientation, and 0.007 for the sagittal orientation. The mean difference in the 15 MV correction factor was 0.008 for the coronal orientation, and 0.006 for the sagittal orientation.

A ratio of the average of each  $32 \times 32$  correction factor to the average of the four central axis (CAX) correction factors at each angle is given in Figures 4.11-4.14. The default correction factors use a single value to correct each ion chamber at a given angle, and that value is taken from the average of the four CAX ion chambers. Figures 4.11-4.14 demonstrate whether the average of the CAX ion chambers is representative of the average of all 1020 ion chambers. For 6 MV, the mean of the ratio of the average to the CAX ion chambers was 1.0070 for the coronal orientation, and 1.0075 for the sagittal orientation. For 15 MV, the mean of the ratio of the average to the CAX ion chambers was 1.0030 for the coronal orientation, and 1.0040 for the sagittal orientation.

## 4.4 CF Verification

### 4.4.1 *Open Arcs*

The results of applying no correction factor, default correction factors, and custom correction factors to open arc fields are shown in Tables 4.4-4.7, evaluated by the percent of pixels passing a gamma criteria of 3%/3mm with a 5% threshold.

### 4.4.2 *Patient Plans*

The results of applying no correction factor, default correction factors, and custom correction factors to 6 and 15 MV patient plans are given in Tables 4.8 and 4.9, evaluated by the percent of pixels passing a gamma criteria of 3%/3mm.

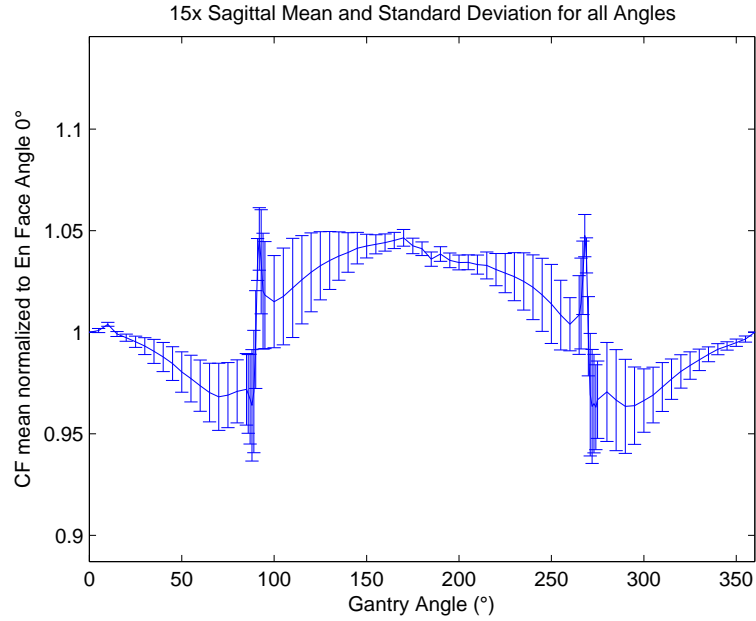


FIGURE 4.6: 15x sagittal CF mean and standard deviation.

Table 4.3: The gantry angles at which the standard deviation  $\sigma > 0.03$  of the correction factors are given for 6 MV coronal and sagittal and 15 MV coronal and sagittal.

Angles with $\sigma > 0.03$			
6 MV Coronal CF	15 MV Coronal CF	6 MV Sagittal CF	15 MV Sagittal CF
87° – 90°		87° – 90°	
93° – 105°	89°	93° – 115°	
115° – 130°	125°	266°	89°
165° – 205°	170° – 175°	270° – 273°	271°
265° – 267°	271°	280° – 290°	
270° – 273°			

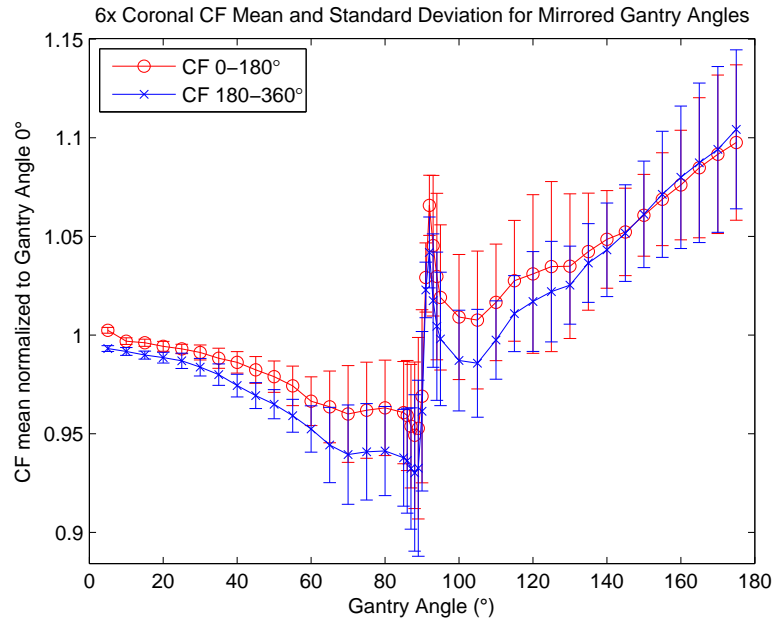


FIGURE 4.7: 6x coronal set-up average and standard deviation of CF for mirrored angles. Gantry angle  $90^\circ$  of CF  $0 - 180^\circ$  corresponds to gantry angle  $270^\circ$  for CF  $180 - 360^\circ$ .

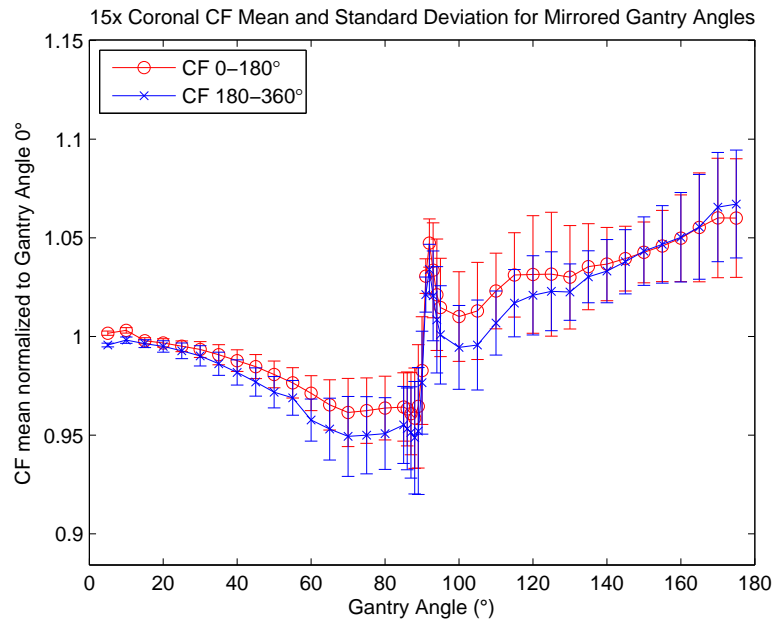


FIGURE 4.8: 15x coronal set-up average and standard deviation of CF for mirrored angles. Gantry angle  $90^\circ$  of CF  $0 - 180^\circ$  corresponds to gantry angle  $270^\circ$  for CF  $180 - 360^\circ$ .

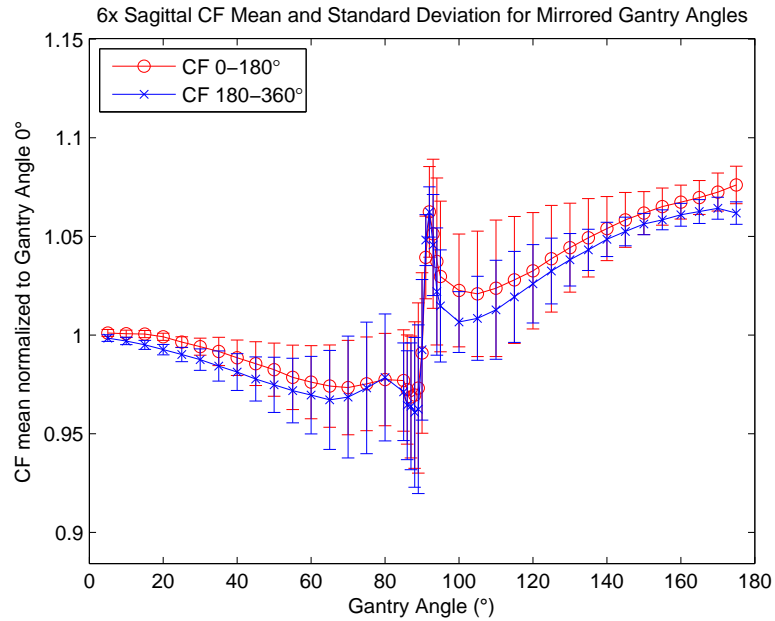


FIGURE 4.9: 6x sagittal set-up average and standard deviation of CF for mirrored angles. Gantry angle  $90^\circ$  of CF  $0 - 180^\circ$  corresponds to gantry angle  $270^\circ$  for CF  $180 - 360^\circ$ .

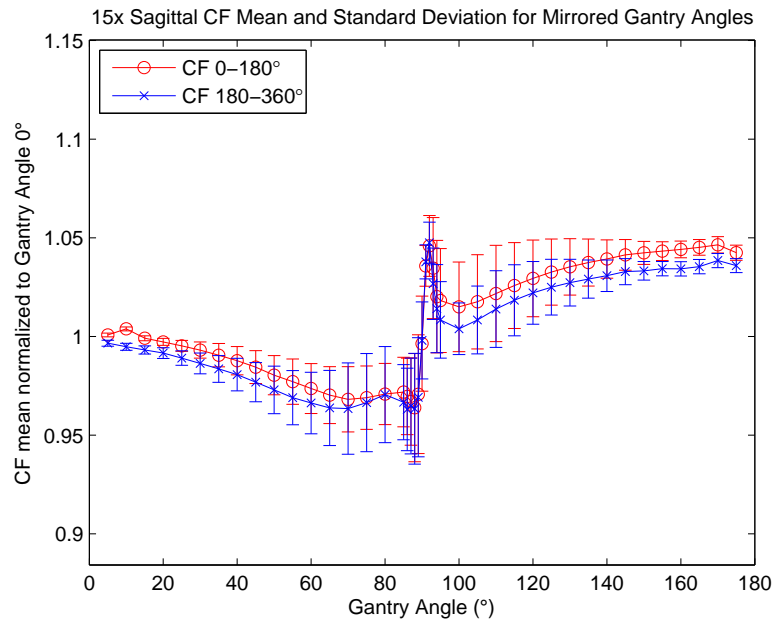


FIGURE 4.10: 15x sagittal set-up average and standard deviation of CF for mirrored angles. Gantry angle  $90^\circ$  of CF  $0 - 180^\circ$  corresponds to gantry angle  $270^\circ$  for CF  $180 - 360^\circ$ .

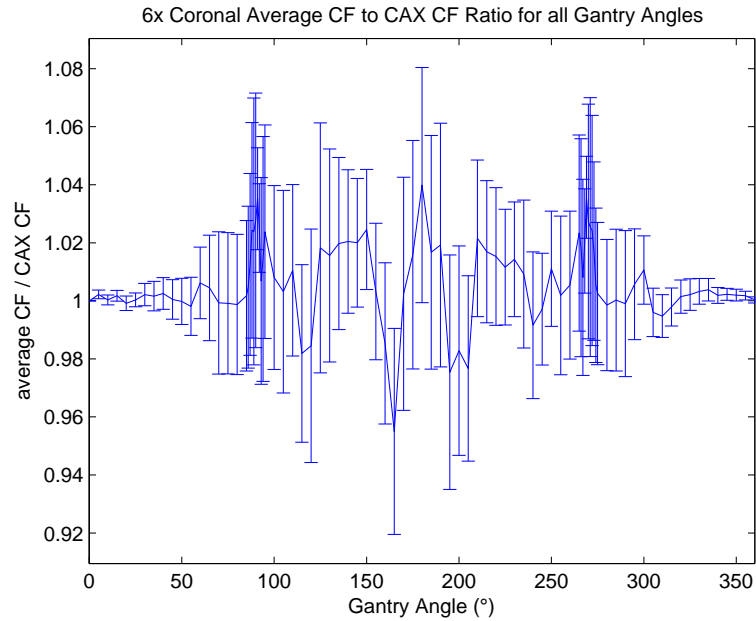


FIGURE 4.11: 6x coronal: At each gantry angle, the ratio of the average of 1024 correction factors to the four central axis (CAX) correction factors is given and the standard deviation for the 6 MV coronal correction factor.

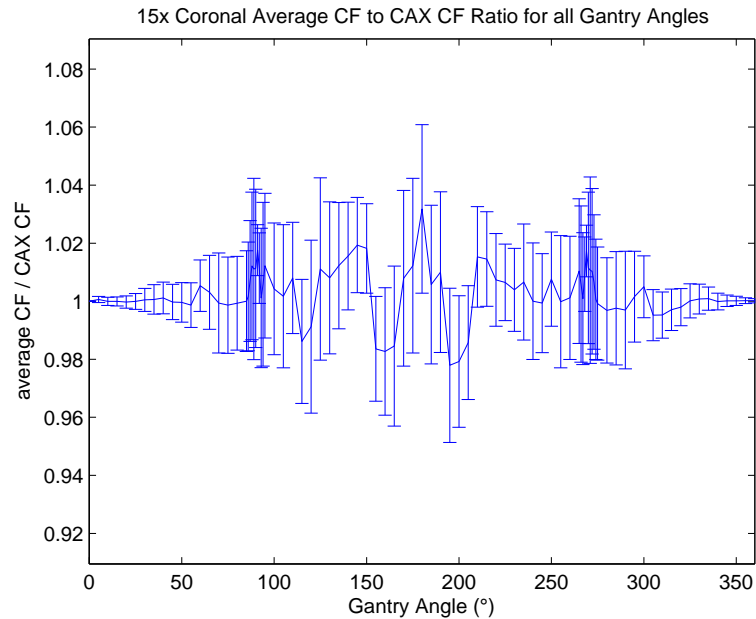


FIGURE 4.12: 15x coronal: At each gantry angle, the ratio of the average of 1024 correction factors to the four central axis (CAX) correction factors is given and the standard deviation for the 15 MV coronal correction factor

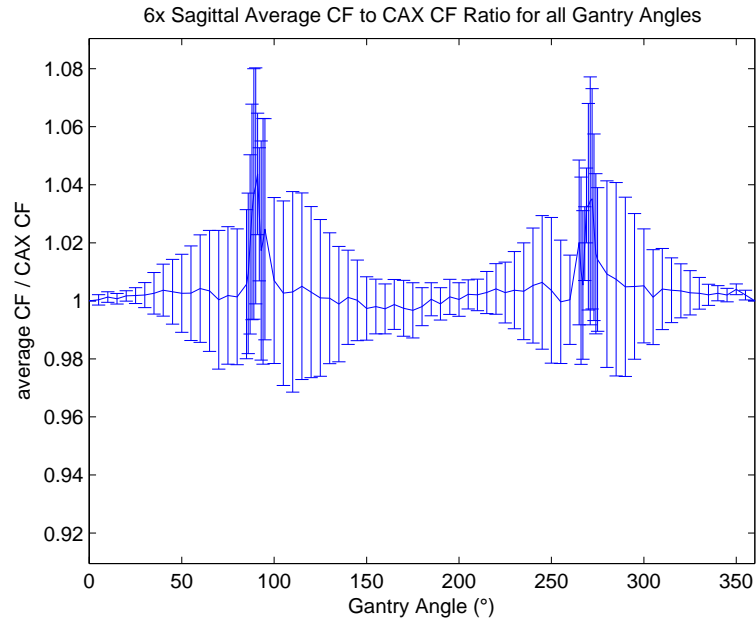


FIGURE 4.13: 6x sagittal: At each gantry angle, the ratio of the average of 1024 correction factors to the four central axis (CAX) correction factors is given and the standard deviation for the 6 MV sagittal correction factor

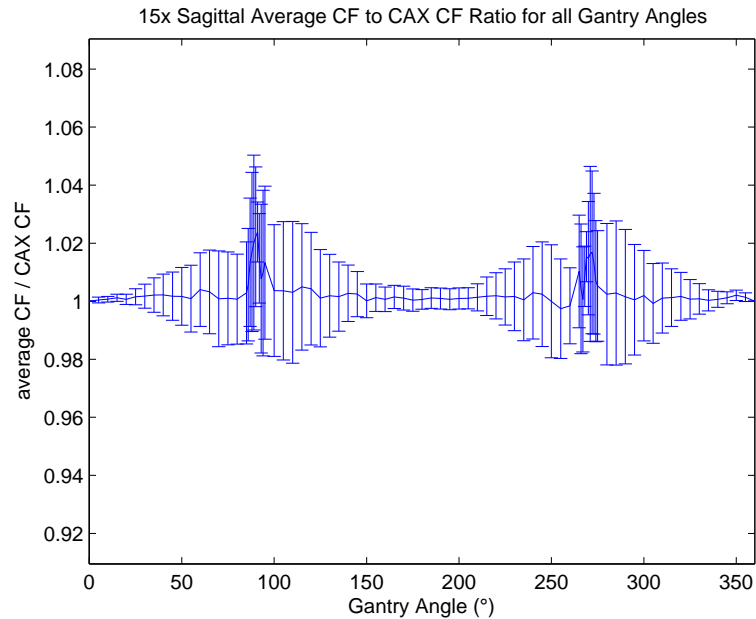


FIGURE 4.14: 15x sagittal: At each gantry angle, the ratio of the average of 1024 correction factors to the four central axis (CAX) correction factors is given and the standard deviation for the 15 MV sagittal correction factor

Table 4.4: CF verification results for 6 MV open fields delivered CCW. The percent of pixels passing a gamma analysis are given when no correction factor is used, when the two manufacturer correction factors are used, and when the two custom correction factors are used on the doses measured by the ICA. N.B. Data collected without background subtraction.

6 MV Analysis CCW					
CCW arcs	180°-135°	135°-45°	45°-315°	315°-225°	225°-180°
No CF	0.1	85.55	96.48	93.36	0.59
180 CF	100	100	99.9	52.25	96.39
360 CF	99.51	92.09	96.58	66.02	97.85
Custom Coronal CF	99.71	99.9	99.9	99.9	99.12
Custom Sagittal CF	98.54	99.8	99.71	99.02	99.8

Table 4.5: CF verification results for 6 MV open fields delivered CW. The percent of pixels passing a gamma analysis are given when no correction factor is used, when the two manufacturer correction factors are used, and when the two custom correction factors are used on the doses measured by the ICA.

6 MV Analysis CW					
CW arcs	180°-135°	135°-45°	45°-315°	315°-225°	225°-180°
No CF	0	86.43	95.61	94.24	0.49
180 CF	100	100	100	53.42	98.24
360 CF	99.51	90.92	95.61	66.02	98.24
Custom Coronal CF	99.71	99.9	99.9	99.8	98.93
Custom Sagittal CF	95.9	99.8	99.71	99.12	100

Table 4.6: CF verification results for 15 MV open fields delivered CCW. The percent of pixels passing a gamma analysis are given when no correction factor is used, when the two manufacturer correction factors are used, and when the two custom correction factors are used on the doses measured by the ICA.

15 MV Percent Passing Gamma Analysis CCW Open Arcs					
CCW arcs	180°-135°	135°-45°	45°-315°	315°-225°	225°-180°
No CF	2.05	99.8	100	99.8	0.2
180 CF	94.04	100	100	99.61	97.85
360 CF	85.35	99.8	100	99.9	81.84
Custom Coronal CF	100	100	100	100	100
Custom Sagittal CF	99.12	100	100	100	97.36

Table 4.7: CF verification results for 15 MV open fields delivered CW. The percent of pixels passing a gamma analysis are given when no correction factor is used, when the two manufacturer correction factors are used, and when the two custom correction factors are used on the doses measured by the ICA.

15 MV Percent Passing Gamma Analysis CW Open Arcs					
CW arcs	180°-135°	135°-45°	45°-315°	315°-225°	225°-180°
No CF	1.95	99.8	100	99.71	0.59
180 CF	92.97	100	100	99.61	98.05
360 CF	84.28	99.8	100	99.9	83.01
Custom Coronal CF	100	100	100	100	100
Custom Sagittal CF	98.93	100	100	100	98.34

Table 4.8: CF verification results for three 6 MV patient plans. The percent of pixels passing a gamma analysis are given when no correction factor is used, when the two manufacturer correction factors are used, and when the two custom correction factors are used on the doses measured by the ICA. N.B. Data gathered without forcing agreement of Eclipse and measurement.

6 MV Patient Plans Gamma Analysis			
Patients	Plan 3	Plan 4	Plan 5
No CF	89.9	86.36	91.88
180 CF	85.77	82.97	81.04
360 CF	88.13	82.65	79.27
Custom Coronal CF	88.71	90.86	84.94
Custom Sagittal CF	86.86	85.99	83.23

Table 4.9: CF verification results for two 15 MV patient plans. The percent of pixels passing a gamma analysis are given when no correction factor is used, when the two manufacturer correction factors are used, and when the two custom correction factors are used on the doses measured by the ICA.

15 MV Patient Plans Gamma Analysis		
Patients	Plan 1	Plan 2
No CF	97.56	95.7
180 CF	91.5	90.72
360 CF	93.46	91.31
Custom Coronal CF	95.31	94.73
Custom Sagittal CF	94.73	95.51

### 5.1 ICA Consistency

By delivering 5 en face fields to the ICA, we found that the ICA shows good consistency of the output of each ion chamber. In addition, the consistency of the ion chambers' response for two distinct photon energies indicates that the ICA response is energy independent for the photon energy ranges used clinically.

### 5.2 Intrinsic MatriXX Response

The delivery of CW and CCW static open fields can be contrasted against the delivery of CW and CCW open field and small field arcs. From the results of the ICA response to static open fields, we found that the average difference in measured readings between CW and CCW deliveries was 0.0 cGy, with a standard deviation of 0.0 cGy for 6 MV fields, and 0.1 cGy for 15 MV fields. On the whole, CW and CCW delivery of static fields does not appear to result in significantly different measurements, which supports our hypothesis that any CCW or CW dependence found in arc fields would be unique to arc delivery.

When CW and CCW open arcs are delivered, the 6 MV arcs showed a slight

increase in the average difference and standard deviation ( $-0.1 \pm 0.2$  cGy), while the 15 MV arc results were no worse than those for the static open fields ( $0.0 \pm 0.1$  cGy). While the difference is measurable, it is too small to make a significant difference in the measurement of clinical treatment fields.

The small field results show a much larger dependence on delivery direction. In particular, the dose in the penumbra region of the narrow fields provides evidence that the direction of delivery effects the magnitude and location of measured dose, as evidenced by the CW-CCW difference map of Figures 4.1 and 4.2. An over-response of chambers in the right side of the field is apparent, compared to an under-response on the left side of the field. As demonstrated in Table 4.1, the narrow fields show a more pronounced CW vs. CCW directional dependence than was observed for open field arcs in the penumbra region of the field. When delivering CCW, starting on the right side of the ICA, delivery began through the high-density layer beneath the chambers. As the arc continued, delivery moved above the high density plane. Upon reaching the left side of the ICA, CCW delivery started above both the chamber and high density material before moving beneath. CW delivery did the opposite. For both 6 MV and 15 MV, the measured dose in the penumbra region was greater when arc delivery began beneath the high density layer. No significant difference was found between  $CCW \rightarrow CW$  vs  $CW \rightarrow CCW$  delivery.

We hypothesize that the demonstrated directional dependence, especially in small fields, might be due to the internal structure of the ICA, in particular to the high density plane situated below the plane of ion chambers as shown in Figure 5.1. As the dose in the penumbra region is affected by the direction of rotation, this may have a significant cumulative effect on VMAT treatment plans which are usually composed of a large number of narrow fields.

The 6 MV and 15 MV static gantry with sliding window MLC fields shows a general trend of increasing agreement between measured and calculated dose with

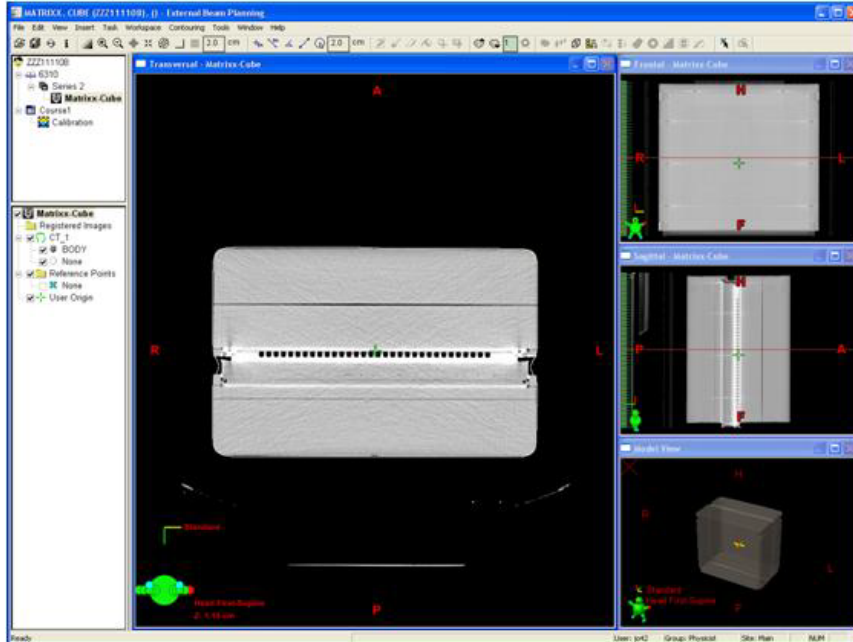


FIGURE 5.1: CT scan of ICA showing plane of ion chambers and high density material plane below.

increasing field size. The 15 MV fields resulted in a greater agreement at each field size than the 6 MV fields. However, in general the agreement was poor, possibly due to the effect of penumbra doses as described above. A possible source for this poor agreement between measured and calculated values is the spatial resolution of the ICA itself. Since the ion chambers are 7.62 mm apart, the radiation from fields less than 7.62 mm will only irradiate one ion chamber, and because the active area of the ion chamber is  $4.5 \times 5(h)$  mm with a chamber volume of  $0.08 \text{ cm}^3$ , the width of the beam may only irradiate a part of the ion chamber. This could result in poor accuracy in the dose measured for small fields. The improved agreement observed with 10 mm fields at both energies may be due to consistent irradiation of at least two ion chambers across the width of the field during irradiation. Future work will include investigation of the source of this effect.

### 5.3 Correction Factor Analysis

In addition to the issue of direction of rotation dependence, the ICA has been shown to have distinct angular dependence[29, 36, 35, 37].

Figures 4.3-4.6 demonstrate the large variability in ion chamber response, in particular as the central axis of the incoming radiation becomes parallel with the ion chamber plane. When the incoming radiation is parallel to the plane of the ion chambers, the photons will mainly pass through the air-filled chambers instead of the water-equivalent build-up material, causing uncertainty in ion chamber response. Additionally, parallel-plate ion chambers are designed to measure radiation that is perpendicular to their orientation, with their effective point of measurement on the front surface of the detector. By changing the orientation of incoming radiation to be parallel to the parallel-plate ion chambers, we are changing the effective point of measurement in an unknown way.

In addition, the figures support the need for a correction factor based on a full 360° measurement, since the values measured are not symmetric around gantry 180°, as shown in Figures 4.7-4.10, and by the results of the paired t-test. In addition, by generating separate coronal and sagittal correction factors, we can examine the effect of the couch on both the correction factor and in its application to arc fields and patient plans. The sagittal correction factors for both 6 MV and 15 MV photons have a smaller average and standard deviation than the coronal correction factors, supporting the hypothesis that fields delivered through the couch are attenuated by the presence of the couch, resulting in much higher standard deviations as shown in the latter half of the 6 MV coronal and sagittal correction factor mirrored plots (Figure 4.7 and Figure 4.9), as well as the comparison of the 15 MV coronal and sagittal correction factors (Figure 4.8 and Figure 4.10) in the 140° – 180 portion of the graphs. The sagittal correction factors have a lower standard deviation through

0° and 180° compared to the coronal results (Figures 4.7-4.10), which must be due purely to angular effects as the sagittal correction factor is not affected by the presence of the couch. Table 4.3 shows the effect of the couch, which increases the number of angles with a large standard deviation, in particular through 180°. Both coronal and sagittal correction factors are subject to any effect created by the high density plane of electronics below the plane of ion chambers, and which may contribute the inherent angular dependent response of the ICA. The default 180CF and 360CF do not include any couch effects.

As well, Figures 4.11-4.14 indicate that the central four ion chambers used to create the default correction factors are not necessarily representative of the average response of all the ion chambers. The sagittal correction factors, which do not include the attenuation introduced by the couch, indicate that the average of the central four ion chambers are within 1 standard deviation of the average of almost all of the ion chambers in the ICA for both 6 MV and 15 MV. The coronal correction factors, which have greater variability as shown previously, demonstrate that the response of the four central ion chambers are less often within a single standard of deviation of the average response the entire ICA than the sagittal correction factors.

The choice of generating and using a custom sagittal versus coronal correction factor resides with the individual physicist but is subject to several considerations. The coronal orientation is simple to set up and measure but the attenuation of the treatment couch can not be removed from the custom-made correction factor. As the patient's true dose will be attenuated by the couch, using a custom coronal correction factor will compensate for the attenuation, concealing the effect from the VMAT QA. Care must be taken if couch attenuation is modeled in the treatment planning system, as using a custom coronal correction factor in conjunction with the calculated dose from the treatment planning system would result in a double correction of attenuation during QA. As well, if the couch uses movable rails then the

custom correction factor would be sensitive to the rail position, potentially leading to errors. The custom sagittal correction factor does not include the attenuation of the couch, removing the complication of hidden couch attenuation and the choice of rail position. However, the set-up requires two orientations (sagittal90 and sagittal270) in order to collect the full 360° measurements.

## 5.4 CF Verification

The verification of the custom coronal and sagittal correction factors using open field and patient plans shows the ability of the correction factors to improve the percent of pixels passing a gamma analysis compared to the default correction factors. For both 6 MV and 15 MV open field arcs, the custom coronal produced the highest passing rates, followed by the custom sagittal. Using no correction factor produced the worst results, in particular for 6 MV. The 6MV default 180° correction factor (180CF) did well between gantry angles 0° – 180°, but not as well for 180° – 360°, in particular around 270°. The default 360° correction factor (360CF) showed similar results to 180CF for 6 MV although results were also somewhat worse around 90°. The default 15 MV 180CF had acceptable results for most angles, but did not do as well from 180° – 135°. The default 15 MV 360CF did well from 225° – 360 and 360° – 135, but performed poorly from 135° – 225°.

The poor results in uncorrected measured dose in open field arcs (Tables 4.4-4.7), in particular for delivery angles which are affected by the couch, demonstrates the possibility of large errors in measurement.

Patient plans showed an interesting trend to have better agreement between measured and calculated dose when no correction factor was applied than when the default or custom correction factors were used. The two custom correction factors showed an improved agreement compared to the default correction factors (with one exception), with the custom coronal correction factors generally showing an improved

agreement compared to the custom sagittal. The default correction factors significantly reduced the passing rate. Overall, not using any CF produced the highest passing rate, and the default correction factors produced the lowest passing rate. This implies that there must be at least one other confounding factor at work during the measurement of VMAT plans. Because the treatment planning system calculated dose agrees with film and ion chamber measurements, it is unlikely that using the treatment planning system as the gold standard in creating the correction factor was the primary source of the complication in VMAT plans. However, it is possible that small changes in the treatment planning system's model of leakage through the MLCs, such as transmission through and scatter from the MLC, may result in improved agreement in VMAT plans. Possible sources of disagreement between measured and calculated dose in VMAT plans require further investigation, and include observations that the ICA underestimates dose for low dose rates and small MU's, while overestimating delivered MU in the case of high dose rates[33]. This observation by Cheong et al. [33] is relevant to VMAT plans, which make use of both high and low dose rates. As well, the cumulative effect of dose in the penumbra region must be examined, as VMAT plans utilize many narrow fields.

# 6

## Conclusion

Our investigation of the angular response of individual ion chambers in the ICA for 6 MV and 15 MV energies has demonstrated significant variation between ion chambers, particularly when the angle of incoming radiation becomes close to parallel with the measurement plane. We also have shown that there is significant asymmetry between angular response for incident radiation from  $0^\circ - 180^\circ$  and  $180^\circ - 360^\circ$ .

The application of the custom correction factors has shown improved agreement between measured and calculated dose for open field arcs. The application of custom correction factors to patient plans resulted in improvement when compared to default custom factors but did not show any significant improvement when compared to not using any correction factor. It is possible that this may be due to a penumbra effect demonstrated with the MLC sliding window results. In addition, we have also shown that the direction of rotation can effect the dose in the penumbra region of small fields, and it is possible that this could have a significant impact on VMAT plans. Future work is needed to ascertain the cause of the lower percent passing observed in VMAT patient plans.

# Appendix A

## Generation of Correction Factors

### A.1 Steps for Creating a Correction Factor File

1. Measured data is copied and pasted from OmniPro software to Excel.
  - (a) Each angle is given its own spreadsheet with the spreadsheet having the angle name (ex. “sheet1” → “270°”). The spreadsheet names can be recycled from previous spreadsheets in order to save the time of typing each name: re-save an old excel file with the correct spreadsheet names as the new file (ie. with a new file name). Select all spreadsheets, and use the option “clear all”. Then copy paste measured data into each blank spreadsheet.
  - (b) If, at the end of a measurement, data is retaken for en-face angle 0° (coronal), 270° (sagittal270), 90° (sagittal90). When the correction factor table is created, the coronal correction factor is given this extra 0° correction factor as the “360°” correction factor entry\*. The sagittal correction factors do not have a place for this duplicate entry, but rather the excel spreadsheet is re-saved to create an “original” sagittal excel file with the

two 270° measurements or two 90° measurement, and a new file is created without the second 270° or 90° measurement. The second file is used to create the correction factor.

2. Calculated data from Eclipse is exported at 100 MU for each angle by right clicking Dose, choosing to export the dose plane, and continuing by choosing a 33×33 point square matrix at 24.384cm in the center of the Matrixx. The 33×33 points will be averaged to a 32×32 point square matrix with MATLAB. Save each DICOM image to a folder that is named for the angle of the DICOM image being exported, eg. “270”.

\*In the case of the coronal measurement, create a 360° DICOM by making a copy of the 0° DICOM (see above for why this is necessary only for the coronal correction factor. Alternatively, if there is no duplicate measurement of the 0° angle in the excel file, the extra DICOM file is not required.).

### 3. MATLAB code

- (a) The first code to run is “rename.m”. This code will renames DICOM images from their default name which is long and ambiguous, and is instead given the same name as their folder name (the name of the angle). It is important to note that this code renames and moves the files up one directory from their original folder. In case something should go wrong, make sure that a copy of the original folders and DICOMS with their original names is saved elsewhere.
- (b) The second code to run is the one that builds the correction factor. The correction factor code is chosen based on the orientation of the ICA and the number of measurements taken (see below).

- i. Since the code that averages multiple experiments (MakeCFtableAverage.m or MakeCFtableAverageSagittal.m) is set up for 3 measurements, it is necessary to edit the code to include more or fewer measurements: 1) in the first cell, make sure that each path to a measurement excel file is given a variable (ex. “one” or “two” etc.), 2) in the same cell, make sure the variable “toAverage” includes all of these directories where

```
toAverage={one, two,...}
```

and 3) in the cell that averages these measurements (the cell where “IMRTarray” is defined), ensure that however many array names are included as correspond to the number of measurements, and that they are divided by the appropriate number of measurements.

- ii. When creating a full 360° sagittal correction factor based on a single 270sagittal and 90sagittal measurement, it is necessary to run makefullsagittalCF.m, which calls both MakeCFtableSagittal.m and MakeCFtable90Sagittal.m. All three m-files must have the first cell variables edited to associate the appropriate file path with given data sets and define variables such as beam energy and beam quality index. For instance, MakeCFtableSagittal.m should have 270sagittal measured and calculated data associated with its variables in the first cell, while MakeCFtable90Sagittal.m should have only 90sagittal data associated with its variables. These two m-files create independent correction factors, which are brought together using makefullsagittalCF.m, where the full correction factor will be output as an excel file.

If creating correction factors using on a single measurement, or averaging

3 data sets, the only changes manually required are generally to specify the directories in the very first cell so that MATLAB will know how to find the excel file and DICOM images, and where to save the correction factor table. When outputting movie files, the cell that contains the movie code may need to be edited to specify the file name and location to which .avi file will be saved.

Individual cells can be evaluated by clicking anywhere inside a cell (the cell turns yellow) followed by the command: `ctrl+enter`. Additionally, right clicking in a cell will also show this command. Multiple cells can be highlighted and evaluated simultaneously using the F9 key. Many of the cells will display both the time it took to evaluate the cell (tic toc function) and display a message to indicate that it finished and a description of the task (ie. “wrote out correction factor” or something similar.)

4. After the correction factors are written to an excel file, the file must be re-saved as a comma separated value file (.csv) in order to be compatible with OmniPro software. When re-saving the excel correction factor table table in .csv format to remove any excess CFs for angles that are not accepted by the OmniPro software (ex.  $>180^\circ$  for certain versions of OmniPro software).

Name	Orientation	Number of measurements
MakeCFtable.m	Coronal	1
MakeCFtableSagittal.m	Sagittal270	1
MakeCFtable90Sagittal.m	Sagittal90	1
makefullsagittalCF.m	Sagittal (full 360°)	1
MakeCFtableAverage	Coronal	more than 1
MakeCFtableAverageSagittal	Sagittal	more than 1

## A.2 Rename Dicom Code

```
1 function rename
2 % Because of the way that the CF code is set up, we need the ...
   dicom files to
3 % be titled '0.dcm' etc. Because eclipse exports them with a ...
   different name
4 % we generally save the dicoms into folders with the appropriate ...
   name of
5 % the angle. Works for both coronal and sagittal data sets.
6
7 % NB. MAKE A COPY OF THE DICOM IMAGES BEFORE YOU START AND SAVE ...
   ELSEWHERE
8 % this is because this code will remove the dcms from their current
9 % location and save them elsewhere so you could lose the ...
   original copy
10 % unless you remember to make a duplicate before hand!
11
12
13 % Here, we obtain the names of these folders from the path below ...
   (the '\\'
14 % is important at the end)
15
16 filepath_dicom='I:\Matrixx\MatrixxEvo-Grey-90Sag-32fs-15x-Copy\';
17
18 originalpath = cd(filepath_dicom);
19 disp('input path')
20 %%
21 % Next, we grab the folders in this directory, and their names
22 dir_dicom=dir(filepath_dicom);
23 names={dir_dicom.name};
24 disp('take names')
25
26 %%
27 %for some reason the first two names are rubbish ( '.' and '..') ...
   so we
28 %start our loop to rename from the third filename
29 for i = 3:(size(names,2))
30 %     for each folder, find the contents (name plus other ...
   attributes)
31     file = dir(strcat(filepath_dicom,names{i}));
32 %     for each file in the folder, pick out the name
33     filename={file.name};
34 %     when you change the name, you completely remove the ...
   original file
35 %     from its current location. MAKE A COPY MANUALLY
36     movefile(strcat(filepath_dicom,names{i}, '/', ...
37                 filename{3}),strcat(filepath_dicom,names{i}, '.dcm'))
```

```
38 end
39 disp('moved files')
```

### A.3 Coronal Correction Factor Code

```
1 function MakeCFtable
2 % For a single coronal measurement
3 tic
4
5 %remember to clearvar
6
7 % define path (dicom image is 33x33 we can use bi-linear ...
   interpolation and
8 % sample corners correctly)
9 filepath_dicom = ...
   'I:\Matrixx\MatrixxEvo-Grey-Coronal-32fs-15x-Copy\';
10
11 % define path (to matrixx data)
12 filename_matrixx_excel = ...
   strcat('I:\Matrixx\CoronalData\GreyCoronal32FS15x',...
13   '\092310\Matrix-Export-Coronal-092310-G0-G360-FS32-GREY-15x');
14
15 % define output path for correction factors (excel file, need ...
   not exist already)
16 filename_cf_norm ...
   =strcat('I:\Matrixx\CoronalData\GreyCoronal32FS15x',...
17   '\092310\cfFS32coronal_normGrey15x-Corners.xls');
18 toc
19
20 %% Obtain data from DICOM images
21 tic
22 % change directory to where the eclipse images are stored
23 originalpath = cd(filepath_dicom);
24 % make structured array of all dicom images in this director
25 dcms=dir('*.dcm');
26
27 % get the names of the dicom images given as: dcms.name
28 % These are not saved in numerical order by angle, so make 3 ...
   cell arrays to
29 % hold variables of different types
30 dcms_order = zeros(1,size(dcms,1));
31 dcms_order2 = cell(1,size(dcms,1));
32 dcms_order_string = cell(1,size(dcms,1));
33
34
35 % since these dcm aren't in the right order: take each filename, ...
   split the
```

```

36 % .dcm off the end, convert the remaining string to a number ...
    ('315' -> 315)
37 for q=1:size(dcms,1)
38     h=strsplit('.dcm', dcms(q).name);
39     dcms_order(1,q)=str2num(h{1});
40 end
41 % once we have all the numbers, we can sort them into the right ...
    order
42 dcms_order=sort(dcms_order);
43 % then we can put make them strings again, put the .dcm back on ...
    the ends.
44 % must use cell array for holding strings
45 for q=1:size(dcms_order,2)
46     dcms_order2{1,q}=num2str(dcms_order(q));
47     g = strcat(dcms_order2{1,q}, '.dcm');
48     dcms_order_string{1,q}=g;
49 end
50 % % print the #.dcm, now in right order
51 % dcms_order_string{:,:};
52
53 % for loop through all dcm files in directory to get the data ...
    associated
54 % with each dcm, save into matrix
55 numdcms = size(dcms,1);
56 all_dcms = zeros(32,32,numdcms);
57 for q = 1:numdcms
58     %     dcms(q).name;
59     % read in dicom image, concatenating strings to get right ...
        file name
60     filename_dicom =strcat(filepath_dicom, dcms_order_string{q});
61     x_uint = dicomread(filename_dicom);
62     % get header info, from which we get the dose grid scaling ...
        (since dicom
63     % put dose into grayscale and we want to go back to dose units
64     xinfo = dicominfo(filename_dicom);
65     scaling = xinfo.DoseGridScaling;
66     %     class(scaling);
67     %     class(x_uint);
68     %since x_uint is an unsigned integer, we need to change the ...
        class to
69     %double or floating point. Otherwise, when we multiply by ...
        the scaling
70     %factor which is a double precision values, we will get very ...
        small
71     %(sub-integer numbers which Matlab would make into 0's in ...
        the array.
72     x = cast(x_uint, 'double');
73     %     class(x); %check that class is changed
74     %     multiply by the scaling factor for dose units, 33x33 matrix
75     dosegrid33 = x*scaling;
76     %     make empty 32x32 matrix

```

```

77     dosegrid32 = zeros(32,32);
78     %average to get 32x32 matrix
79     for xval=1:32
80         for yval=1:32
81             dosegrid32(xval,yval) = (dosegrid33(xval,yval)+...
82                 dosegrid33((xval+1),yval)+dosegrid33(xval,(yval+1))+...
83                 dosegrid33((xval+1),(yval+1)))/4;
84         end
85     end
86     all_dcms(:, :, q)=dosegrid32;
87     clearvars dosegrid32 dosegrid33
88 end
89 toc
90
91 %% Obtain data from Matrixx images
92 tic
93 % return to original matlab folder directoy which contains ...
94     function files I
95 % call here and later
96 cd(originalpath)
97 % This section will take the matrixx data from excel and import ...
98     the data to
99 % Matlab for analysis (alternative command (uiimport)
100
101 % Find the names of the spreadsheets (contained in 'desc').
102 [typ, desc] = xlsfinfo(filename_matrixx_excel);
103 % Find the number of spreadsheets in the file
104 sheetnumber = size(desc,2);
105 % Import, giving file name, sheet name, and upper left to bottom ...
106     right
107 % cells of interest (can only take a rectangular array of data).
108
109 % Desc holds the sheets names in a cell array, class = cell. ...
110     Unfortunately
111 % 'xlsread' cannot pick out desc(1) as a string without help so ...
112     we need to
113 % change the class using 'cellstr'.
114 sheet = cellstr(desc);
115 % Create stacked (#Dimensions) matrix array to hold each matrix ...
116     (from each
117 % excel sheet). Call this IMRT array since obtained at static ...
118     gantry angles
119 IMRTarray = zeros(32,32,sheetnumber);
120 % Grab each spreadsheet in the workbook (assumes all ...
121     spreadsheets have
122 % information in them that we want and we want the same cells ...
123     from every
124 % spreadsheet).
125 for i = 1:sheetnumber
126     IMRTarray(:, :, i) = ...

```

```

119         xlsread(filename_matrixx_excel, sheet{i}, 'B32:AG64');% ...
            dose data
120     [text,num]= ...
121         xlsread(filename_matrixx_excel, sheet{i}, 'A16');% data ...
            factor
122 % A16 cell data factor is not a number, so split off string ...
    part to
123 % get #
124     header = regexp(cast(num,'char'),' ','split');
125     scale = str2num(char(header(2)));
126 % multiply by scale, and divide to get units of gray
127     IMRTarray(:, :, i)=IMRTarray(:, :, i)*scale/1000;
128 end
129 toc
130 %% Make CF table!
131 tic
132 % make CF table by dividing calc/meas (or eclipse/measured)
133 % check that data is the same size from IMRT data (matrixx) and ...
    dicom
134 angles = size(all_dcms,3);
135 % if not equal, print error message
136 if size(IMRTarray,3) ≠ size(all_dcms,3)
137     disp('the number of angles for comparison do not match')
138     for i=1:size(all_dcms,3)
139         if dcms_order(i) ≠ str2num(sheet{i})
140             dcms_order(i)
141         end
142     end
143 elseif size(IMRTarray,3) == size(all_dcms,3)
144     cf_table = zeros(32,32,angles);
145 %     for comparison, what does this look like without corner ...
    correction?
146     cf_table_noC = zeros(32,32,angles);
147     for h = 1:angles
148         cf_table(:, :, h) = all_dcms(:, :, h)./IMRTarray(:, :, h);
149 %         cf_table_noC(:, :, h) = ...
    all_dcms(:, :, h)./IMRTarrayOld(:, :, h);
150     end
151 end
152
153 % make vector containing names of the angles in order
154 all_angles = zeros(1,numdcms);
155 for g =1:size(sheet,2)
156 all_angles(:,g)=str2num(sheet{g});
157 end
158 toc
159 %% Normalize CF table to G0
160 tic
161 sx=size(cf_table);
162 norm_cf_g0 = cf_table./repmat(cf_table(:, :, 1), [1 1 sx(3:end)]);
163 disp('normalized CF to G0')

```

```

164 %% interp corners
165 cd('I:/Matrixx/Matlab')
166 norm_cf_g0_orig = norm_cf_g0;
167 norm_cf_g0_corners=zeros(size(norm_cf_g0_orig));
168 % interpolate corners
169 for i = 1:sheetnumber
170     norm_cf_g0_C = interp_corners(norm_cf_g0_orig(:, :, i)) ;
171     norm_cf_g0_corners(:, :, i)=norm_cf_g0_C;
172 end
173 disp('interp corners')
174
175 %% write norm CF Table to excel file, remember to resave as .csv!
176 % ALSO, choose appropriate beam energy and BQI (see below)
177
178 % make place holder to write initially to excel file
179 M=0;
180 numberangles = size(all_angles,2);
181 xlswrite(filename_cf_norm, M)
182 % pause(1.5)
183 promptforsave=0;
184
185 % write angle name, followed by CF 32x32 matrix in loop
186 for i = 1:numberangles
187 Write2Excel(filename_cf_norm,promptforsave,...
188     strcat('A', num2str(3+33*(i-1))), norm_cf_g0_corners(:, :, i))
189 Write2Excel(filename_cf_norm,promptforsave,...
190     strcat('A', num2str(2+33*(i-1))), all_angles(1,i))
191 end
192 Write2Excel(filename_cf_norm,promptforsave,'A1',{'Linac: Varian ...
193     2100C'})
194 % BeamEnergy = '15';
195 % BeamQualityIndex = '0.7598';
196 BeamEnergy = '6';
197 BeamQualityIndex = '0.6767';
198 Write2Excel(filename_cf_norm,promptforsave,'B1',{BeamEnergy})
199 Write2Excel(filename_cf_norm,promptforsave,'C1',{BeamQualityIndex})
200 Write2Excel(filename_cf_norm,promptforsave,'D1',{32})
201 Write2Excel(filename_cf_norm,promptforsave,'E1',{32})
202 disp('remember to resave excel file as .csv!')
203 toc
204
205 %% Make 2 plots:
206
207 % Plot #1: error bars 2D line plot mean and standard deviation ...
208 % of CF normalized
209 stdev=zeros(sheetnumber,1);
210 average=zeros(sheetnumber,1);
211
212 % mean measured data set at each angle
213 average=mean(mean(norm_cf_g0_corners));
214 % unfortunately, we can't just take std(std(...)), so we ...
215 % need to break

```

```

212 %     it up into matrices that we want to act on
213     for f = 1:sheetnumber
214         b=norm_cf_g0_corners(:, :, f);
215         stdev(f)=std(b(:));
216     end
217 figure(1)
218 errorbar(all_angles, average, stdev)
219 axis tight
220 % want axis to match 6x coronal so all plot comparable
221 axis([0 360 0.8870 1.1455])
222 ylabel(['CF mean normalized to Gantry Angle 0' setstr(176) ])
223 xlabel(['Gantry Angle (' setstr(176) ')'])
224 title('15x Coronal Mean and Standard Deviation for all Gantry ...
        Angles')
225
226
227 % Plot #2: Same data but mirrored from 0-180
228
229 average180 = squeeze(average(2:44));
230 average360 = flipud(squeeze(average(46:end-1)));
231 std180 = squeeze(stdev(2:44));
232 std360 = flipud(squeeze(stdev(46:end-1)));
233 figure(2)
234 errorbar(all_angles(2:44), average180, std180, '-r*')
235 hold on
236 errorbar(all_angles(2:44), average360, std360, '-bx')
237 axis tight
238 % axis([0 180 min(average)-max(stdev) max(average)+max(stdev)])
239 % for anything not 6x coronal, we want axes to match 6x coronal
240 axis([0 180 0.8842 1.1502])
241 ylabel(['CF mean normalized to Gantry Angle 0' setstr(176) ])
242 xlabel(['Gantry Angle (' setstr(176) ')'])
243 title('6x Coronal CF Mean and Standard Deviation for Mirrored ...
        Gantry Angles')
244 legend('CF 0-180\circ', 'CF 180-360\circ', 'location', 'NorthWest')
245 hold off
246 %% Make plot of ave/CAX 4 ion chambers, and stdev
247 % grab all four central ion chamber values
248 cax1 = squeeze(norm_cf_g0_corners(16,16,:));
249 cax2 = squeeze(norm_cf_g0_corners(16,17,:));
250 cax3 = squeeze(norm_cf_g0_corners(17,16,:));
251 cax4 = squeeze(norm_cf_g0_corners(17,17,:));
252 % average the values to get 89 averaged CAX values
253 cax=(cax1+cax2+cax3+cax4)/4;
254 % take the 89 averaged values and divide by 89 cax values
255 CFtoCAX = squeeze(average)./cax;
256 figure(1)
257 errorbar(all_angles, CFtoCAX, stdev)
258 axis tight
259 axis([0 360 (0.9195-0.01) (1.0804+0.01)])
260 ylabel('average CF / CAX CF')

```

```

261 xlabel(['Gantry Angle (' setstr(176) ')'])
262 title('15x Coronal Average CF to CAX CF Ratio for all Gantry ...
        Angles')
263 max(CFtoCAX)
264 mean(CFtoCAX)
265
266 %% Paired Angles
267
268 % Grab the paired angles and compare using a paired t-test
269 % (don't use 0,180, or 360 degree angles)
270
271 % Start with the average variable calculated in the last cell!
272
273 % all_angles(2:44)
274 average180 = squeeze(average(2:44));
275 average360 = flipud(squeeze(average(46:end-1)));
276
277 CF180 = norm_cf_g0_corners(:, :, 2:44);
278 CF360 = norm_cf_g0_corners(:, :, 46:end-1);
279 [h,p]=ttest(CF180,CF360,0.05,'both',3);
280 %% find angles with st dev > 0.03 and >0.05
281 stdev3=(all_angles(find(stdev>0.03))');
282 stdev5=(all_angles(find(stdev>0.05))');
283 all_angles(stdev==(max(stdev)))
284 %% make CF movie for export: Make sure to include director where ...
        movie
285 % should be saved when calling the avifile function below
286
287 % make movie of correction factors
288 tic
289 fig2=figure(2);
290 set(fig2,'Renderer','ZBuffer');
291 rect=get(fig2, 'Position');
292 rect(1:2)=[0 0];
293 nframes = size(norm_cf_g0_corners,3);
294 M=moviein(nframes);
295 set(fig2, 'nextplot', 'replacechildren');
296 mn_cf = min(min(min(norm_cf_g0_corners)));
297 mx_cf = max(max(max(norm_cf_g0_corners)));
298 axis([0 32 0 32 mn_cf mx_cf]);
299 ax=axis;
300 axis manual
301 colormap(winter)
302 aviobj = avifile(...
303     'I:\Matrixx\MatrixxResearchMovies2\CF15xCor.avi', ...
        'compression','none', 'fps',2);
304 % stdevmov=avifile('H:\MatrixxResearchMovies\stdev.avi', 'fps', ...
        0.5);
305
306 for i = 1:size(norm_cf_g0_corners,3)
307     %     pause(1)

```

```

308     surf(norm_cf_g0_corners(:, :, i));
309     colorbar
310     axis(ax)
311     caxis([mn_cf mx_cf])
312     title(strcat(...
313         'Correction Factor for Gantry Angle: ', ...
314         num2str(all_angles(1,i)), '\circ'))
314     zlabel('CF')
315     pause(0.5)
316     M(:, i)=getframe(fig2, rect);
317 %     stdevmov=addframe(stdevmove, M);
318     aviobj = addframe(aviobj, M(i));
319 end
320 map=colormap;
321 aviobj=close(aviobj);
322 disp('made movie')
323 toc
324 %%
325 clear

```

## A.4 Sagittal Correction Factor Code

Due to the two distinct sagittal orientations used to create the sagittal correction factor, the MATLAB code that follows is divided into three parts. Sections A.4.1 and A.4.2 create the correction factors for data acquired from the sagittal 270 and sagittal90 orientations respectively. Section A.4 provides the code which brings both sets of correction factors together and organizes them into a single set sagittal correction factors.

```

1 %% IMPORTANT: this m-file calls MakeCFtableSagittal and ...
  MakeCFtable90Sagittal.
2 % It is important to update the first cell in each of these with ...
  the path
3 % and file names that we need to make the total CF, as well as ...
  update this
4 % cell with energy and BQI values
5 filename_totalcfsag = ...
  'I:\Matrixx\CF\totalsagNORMCF6xGrey-Corners.xls';
6 BeamEnergy = '6';
7 % BeamEnergy = '15';
8 BeamQualityIndex = '0.6767';
9 % BeamQualityIndex = '0.7598';

```

```

10 %% call two function to make 270 and 90 CFs independently, and ...
    already
11 % normalized
12 [norm_cf270, allangles270sag] = MakeCFtableSagittal;
13 [norm_cf_90sag, allangles90sag] = MakeCFtable90Sagittal;
14 % we will have repeat data for 180 and 0 degrees, so we will ...
    average there
15 %% First, reorder each for equivalent coronal order
16 % reordering 270 and 90 sag angles
17 [v,ia,ib]=intersect(allangles90sag, sort(allangles90sag(2:end)));
18 norm_cf90=zeros(size(norm_cf_90sag));
19 norm_cf90(:, :, 1:(end-1)) = norm_cf_90sag(:, :, ia);
20 norm_cf90(:, :, end)=norm_cf_90sag(:, :, 1);
21 % now 90sag is organized from CF180 to CF270 to CF0
22 % 270sag already organized from CF0 to CF90 to CF180
23 % now we can put them together in new matrix, but average the ...
    two angles
24 % that overlap (CF0 and CF180)
25 % make array to hold both data sets
26 norm_cf_totalsag = ...
    zeros(32,32,(size(norm_cf90,3)+size(norm_cf270,3)-2));
27 % put in CF 0 to CF 180
28 norm_cf_totalsag(:, :, (1:size(norm_cf270,3))) = norm_cf270;
29 % average the CF 0 and CF 180 from 90sag to the ones we just put in
30 norm_cf_totalsag(:, :, 1) = ...
    (norm_cf_totalsag(:, :, 1)+norm_cf90(:, :, end))/2;
31 norm_cf_totalsag(:, :, 45) = ...
    (norm_cf_totalsag(:, :, 45)+norm_cf90(:, :, 1))/2;
32 % now put in the rest of the 90sags
33 norm_cf_totalsag(:, :, ((size(norm_cf270,3))+1):end) = ...
    norm_cf90(:, :, (2:end-1));
34 %% correct corners by averaging
35 all_angles = [allangles270sag,allangles90sag(ia(2:end))];
36 norm_cf_totalsag_orig = norm_cf_totalsag;
37 norm_cf_totalsag_corners=zeros(size(norm_cf_totalsag_orig));
38 % interpolate corners
39 for i = 1:size(norm_cf_totalsag_orig,3)
40     norm_cf_totalsag_C = ...
        interp_corners(norm_cf_totalsag_orig(:, :, i)) ;
41     norm_cf_totalsag_corners(:, :, i)=norm_cf_totalsag_C;
42 end
43 %% want to duplicate the 0 value as the 360 value
44 % (currently ranges from 0-355)
45 % and add that on to both all_angles and norm_cf_totalsag_corners
46 norm_cf_totalsag_corners(:, :, ...
    end+1)=norm_cf_totalsag_corners(:, :, 1);
47 all_angles(end+1)=360;
48
49 %% now we can save this to excel, but remember to resave as .csv
50 size(norm_cf_totalsag)
51 M = 0;

```

```

52  xlsxwrite(filename_totalcfSAG, M)
53  % pause(1.5)
54  promptforsave=0;
55  for i = 1:size(norm_cf_totalsag_corners,3)
56  Write2Excel(filename_totalcfSAG,promptforsave,...
57      strcat('A', num2str(3+33*(i-1))), ...
          norm_cf_totalsag_corners(:, :, i))
58  Write2Excel(filename_totalcfSAG,promptforsave,...
59      strcat('A', num2str(2+33*(i-1))), all_angles(1,i))
60  end
61  Write2Excel(filename_totalcfSAG,promptforsave, 'A1', {'Linac: ...
          Varian 2100C'})
62  Write2Excel(filename_totalcfSAG,promptforsave, 'B1', {BeamEnergy})
63  Write2Excel(filename_totalcfSAG,promptforsave, 'C1', {BeamQualityIndex})
64  Write2Excel(filename_totalcfSAG,promptforsave, 'D1', {32})
65  Write2Excel(filename_totalcfSAG,promptforsave, 'E1', {32})
66  %% make movie for export (note that scaling should be chosen below
67  % depending on energy, so that the scaling is comparable to the
68  % coronal scaling!
69  tic
70  fig2=figure(2);
71  set(fig2, 'Renderer', 'ZBuffer');
72  rect=get(fig2, 'Position');
73  rect(1:2)=[0 0];
74  nframes = size(norm_cf_totalsag_corners,3);
75  M=moviein(nframes);
76  set(fig2, 'nextplot', 'replacechildren');
77  % mn_cf = min(min(min(norm_cf_totalsag_corners)));
78  % mx_cf = max(max(max(norm_cf_totalsag_corners)));
79  % % 6x- because we want to the scaling to be the same as the coronal
80  % mx_cf = 1.2384;
81  % mn_cf = 0.8417;
82  % % 15x- because we want to the scaling to be the same as the ...
          coronal
83  mx_cf = 1.1626;
84  mn_cf = 0.8824;
85  axis([0 32 0 32  mn_cf mx_cf]);
86  ax=axis;
87  axis manual
88  colormap(winter)
89  aviobj=avifile...
90  ('I:\Matrixx\MatrixxResearchMovies2\CF15xSagittal.avi', ...
          'compression', 'none', 'fps', 2);
91  % stdevmov=avifile('H:\MatrixxResearchMovies\stdev.avi', 'fps', ...
          0.5);
92  for i = 1:size(norm_cf_totalsag_corners,3)
93  %     pause(1)
94      surf(norm_cf_totalsag_corners(:, :, i));
95      colorbar
96      axis(ax)
97      caxis([mn_cf mx_cf])

```

```

98     title(strcat...
99         ('Correction Factor for Gantry Angle: ', ...
100            num2str(all_angles(1,i)), '\circ'))
101     xlabel('CF')
102     pause(0.5)
103     M(:,i)=getframe(fig2,rect);
104     %   stdevmov=addframe(stdevmove, M);
105     aviobj = addframe(aviobj,M(i));
106 end
107 map=colormap;
108 aviobj=close(aviobj);
109 disp('made movie')
110 %% Make 2 plots:
111 %Plot1: error bars 2D line plot mean and standard deviation of ...
112         CF normalized
113 sheetnumber = size(norm_cf_totalsag_corners,3);
114 stdev=zeros(sheetnumber,1);
115 average=zeros(sheetnumber,1);
116
117 % mean measured data set at each angle
118 average=mean(mean(norm_cf_totalsag_corners));
119 %   unfortunately, we can't just take std(std(...)), so we ...
120 %   need to break
121 %   it up into matrices that we want to act on
122 for f = 1:sheetnumber
123     b=norm_cf_totalsag_corners(:, :, f);
124     stdev(f)=std(b(:));
125 end
126 figure(1)
127 errorbar(all_angles,average,stdev)
128 axis tight
129 % want axis to match 6x coronal so all plots comparable
130 axis([0 360 0.8870 1.1455])
131 ylabel(['CF mean normalized to En Face Angle 0' setstr(176) ])
132 xlabel(['Gantry Angle (' setstr(176) ')'])
133 title('6x Sagittal Mean and Standard Deviation for all Angles')
134
135 average180 = squeeze(average(2:44));
136 average360 = flipud(squeeze(average(46:end-1)));
137 std180 = squeeze(stdev(2:44));
138 std360 = flipud(squeeze(stdev(46:end-1)));
139 figure(2)
140 errorbar(all_angles(2:44), average180,std180, '-r*')
141 hold on
142 errorbar(all_angles(2:44), average360,std360, '-bx')
143 axis tight
144 % % axis([0 180 min(average)-max(stdev) max(average)+max(stdev)])
145 % for anything not 6x coronal, we want axes to match 6x coronal
146 axis([0 180 0.8842 1.1502])
147 ylabel(['CF mean normalized to Gantry Angle 0' setstr(176) ])
148 xlabel(['Gantry Angle (' setstr(176) ')'])

```

```

146 title('6x Sagittal CF Mean and Standard Deviation for Mirrored ...
        Gantry Angles')
147 legend('CF 0-180\circ', 'CF 180-360\circ', 'location', 'NorthWest')
148 hold off
149 %% find ave/CAX ion chamber with stdev
150 % grab all four central ion chamber values
151 cax1 = squeeze(norm_cf_totalsag_corners(16,16,:));
152 cax2 = squeeze(norm_cf_totalsag_corners(16,17,:));
153 cax3 = squeeze(norm_cf_totalsag_corners(17,16,:));
154 cax4 = squeeze(norm_cf_totalsag_corners(17,17,:));
155 % average the values to get 89 averaged CAX values
156 cax=(cax1+cax2+cax3+cax4)/4;
157 % take the 89 averaged values and divide by 89 cax values
158 CFtoCAX = squeeze(average)./cax;
159 figure(1)
160 errorbar(all_angles,CFtoCAX,stdev)
161 axis tight
162 % scale must be the same on coronal and sagittal figures
163 axis([0 360 (0.9195-0.01) (1.0804+0.01)])
164 ylabel('average CF / CAX CF')
165 xlabel(['Gantry Angle (' setstr(176) ')'])
166 title('6x Sagittal Average CF to CAX CF Ratio for all Gantry ...
        Angles')
167 max(CFtoCAX)
168 mean(CFtoCAX)
169 %% Paired Angles
170 % Grab the paired angles and compare using a paired
171 % t-test (don't want 0,180, or 360 degree angles)
172 % Start with the average variable calculated in the last cell!
173 % all_angles(2:44)
174 average180 = squeeze(average(2:44));
175 % fliplr(all_angles(46:end-1));
176 average360 = flipud(squeeze(average(46:end-1)));
177 CF180 = norm_cf_totalsag_corners(:, :, 2:44);
178 CF360 = norm_cf_totalsag_corners(:, :, 46:end-1);
179 CF360 = flipdim(CF360, 3);
180 [h,p]=ttest(CF180,CF360,0.05,'both',3);
181 surface(p)
182 colormap('winter')
183 colorbar
184 axis image
185 title('15x sagittal p values')
186 %% find angles with st dev > 0.03 and >0.05
187 stdev3=(all_angles(find(stdev>0.03)))';
188 stdev5=(all_angles(find(stdev>0.05)))';
189 all_angles(stdev==(max(stdev)))

```

#### A.4.1 Sagittal270 Correction Factor Code

```

1 function [norm_cf270, all_angles] = MakeCFtableSagittal
2 % for single 270sagittal measurement, make CF
3 tic
4 %remember to clearvar
5
6 % define path (dicom image is 33x33 we can use bi-linear ...
   interpolation and
7 % sample corners correctly)
8 filepath_dicom = 'I:\Matrixx\MatrixxEvo-Sagittal-32fs-Copy\';
9 % define path (to matrixx data)
10 filename_matrixx_excel = ...
   strcat('I:\Matrixx\SagittalData\32FS\051510',...
11        '\Matrix-Export-Sagittal-051510-G270-G90-FS32-GREY');
12 % Make sure these are right
13 BeamEnergy = '6';
14 % % for 6x BQI is...
15 BeamQualityIndex = '0.6767';
16 % % for 15x BQI is...
17 % BeamQualityIndex = '0.7598';
18 disp('input file names')
19 toc
20 %% Get DICOM data
21 tic
22 % change directory to where the eclipse images are stored
23 originalpath = cd(filepath_dicom);
24 % make structured array of all dicom images in this director
25 dcms=dir('*.dcm');
26 % get the names of the dicom images
27 % dcms.name
28 % fix the order of dcm names
29 % make cell arrays to hold everything
30 dcms_order = zeros(1,size(dcms,1));
31 dcms_order2 = cell(1,size(dcms,1));
32 dcms_order_string = cell(1,size(dcms,1));
33 % since these aren't in the right order we take each filename, ...
   split the
34 % .dcm off the end, convert the remaining string to a number ...
   ('315'->315)
35 for q=1:size(dcms,1)
36     h=strsplit('.dcm', dcms(q).name);
37     dcms_order(1,q)=str2num(h{1});
38 end
39 % once we have all the numbers, we can sort them into the right ...
   order
40 radians=sin(dcms_order*pi/180);
41 dcms_new_order=sort(radians);
42 [valuessag, iasag, ...
   ibsag]=intersect(sin(dcms_order*pi/180),dcms_new_order);
43 dcms_order(iasag);
44 % then we can put make them strings again, put the .dcm back on ...
   the ends.

```

```

45 % must use cell array for strings
46 for q=1:size(dcms_order,2)
47     dcms_order2{1,q}=num2str(dcms_order(iasag(q)));
48     g = strcat(dcms_order2{1,q}, '.dcm');
49     dcms_order_string{1,q}=g;
50 end
51 % for loop through all dcm files in directory, interpolating and ...
    putting
52 % them in to array in proper order
53 numdcms = size(dcms,1);
54 all_dcms = zeros(32,32,numdcms);
55 for q = 1:numdcms
56     % read in dicom image, concatenating strings to get right ...
        file name
57     filename_dicom =strcat(filepath_dicom, dcms_order_string{1,q});
58     x_uint = dicomread(filename_dicom);
59     % get header info, from which we get the dose grid scaling ...
        (since dicom
60     % put dose into grayscale and we want to go back to dose
61     xinfo = dicominfo(filename_dicom);
62     scaling = xinfo.DoseGridScaling;
63     class(scaling);
64     class(x_uint);
65     %since x_uint is an unsigned integer, we need to change the ...
        cclass to
66     %double or floating point. Otherwise, when we multiple by ...
        the scaling
67     %factor which is a double precision values, we will get very ...
        small
68     %(sub-integer numbers which Matlab would make into 0's in ...
        the array.
69     x = cast(x_uint, 'double');
70     class(x);
71     dosegrid33 = x*scaling;
72     size(dosegrid33);
73     dosegrid32 = zeros(32,32);
74     %average to get 32x32
75     for xval=1:32
76         for yval=1:32
77             dosegrid32(xval,yval) = (dosegrid33(xval,yval)+...
78                 dosegrid33((xval+1),yval)+dosegrid33(xval,(yval+1))+...
79                 dosegrid33((xval+1),(yval+1)))/4;
80         end
81     end
82     all_dcms(:, :, q)=dosegrid32;
83     clearvars dosegrid32 dosegrid33
84 end
85 disp('got dicom images in format required')
86 toc
87 %% Get Matrixx data
88 tic

```

```

89 % return to original matlab folder directoy which contains ...
    function files I
90 % call here and later
91 cd(originalpath)
92 % This section will take the IMRT (Matrixx data from static ...
    fields) data
93 % from excel and import the data to Matlab for analysis
94 % Find the names of the spreadsheets (contained in 'desc').
95 [typ, desc] = xlsfinfo(filename_matrixx.excel);
96 % Find the number of spreadsheets in the file
97 sheetnumber = size(desc,2);
98 % Import, giving file name, sheet name, and upper left to bottom ...
    right
99 % cells of interest (can only take a rectangular array of data).
100 % Desc holds the sheets names in a cell array, class = cell. ...
    Unfortunately
101 % 'xlsread' cannot pick out desc(1) as a string without help so ...
    we need to
102 % change the class using 'cellstr'.
103 sheet = cellstr(desc);
104 class(sheet);
105 size(sheet);
106 % Create stacked (#Dim) matrix array to hold each matrix (from ...
    each sheet).
107 IMRTarray = zeros(32,32,sheetnumber);
108 % Grab each spreadsheet in the workbook (assumes all ...
    spreadsheets have
109 % information in them that we want and we want the same cells every
110 % spreadsheet).
111 for i = 1:sheetnumber
112     IMRTarray(:, :, i) = xlsread(filename_matrixx.excel, sheet{i}, ...
        'B32:AG64');
113     % need data factor
114     [text,num]= xlsread(filename_matrixx.excel, sheet{i}, 'A16');
115     header=regexp(cast(num,'char'),' ','split');
116     scale = str2num(char(header(2)));
117     %multiply by scale, and divide to get units of gray
118     IMRTarray(:, :, i)=IMRTarray(:, :, i)*scale/1000;
119 end
120 toc
121 %% make CF table by dividing calc/meas (or eclipse/measured)
122 tic
123 % check that data is the same size from IMRT data (matrixx) and ...
    dicom
124 angles = size(all_dcms,3);
125 % if not equal, print error message
126 if size(IMRTarray,3) ≠ size(all_dcms,3)
127     disp('THE NUMBER OF ANGLES FOR COMPARISON DO NOT MATCH!')
128 elseif size(IMRTarray,3) == size(all_dcms,3)
129     cf_table270 = zeros(32,32,angles);
130     for h = 1:angles

```

```

131         cf_table270(:, :, h) = all_dcms(:, :, h) ./ IMRTarray(:, :, h);
132     end
133 end
134 disp('made cf table')
135 toc
136 t(1,4)=toc;
137 all_angles = [0:5:85, 86:1:94, 95:5:180];
138 toc
139 %% Normalize CF table to G270
140 tic
141 sx=size(cf_table270);
142 norm_cf270 = cf_table270 ./ repmat(cf_table270(:, :, 1), [1 1 ...
        sx(3:end)]);
143 toc
144 %%
145 % clear

```

#### A.4.2 Sagittal90 Correction Factor Code

```

1 function [norm_cf_90sag, all_angles] = MakeCFtable90Sagittal
2 %The difference between this m.file and MakeCFtable.m is that ...
   this one
3 %will make a CF table for 90 sagittal alone
4 tic
5 %remember to clearvar
6
7 % define path (dicom image is 33x33—we can use bi-linear ...
   interpolation and
8 % sample corners correctly)
9 filepath_dicom = 'I:\Matrixx\MatrixxEvo-Blue-90Sag-32fs-6x-Copy\';
10
11 % define path for excel (matrix) data
12 filename_matrix_excel = strcat('I:\Matrixx\SagittalData\90SAG', ...
13     '\GreySag6x32FS', ...
14     '\Matrix-Export-90Sagittal-092310-G90-G270-FS32-GREY-6x');
15
16 % remember to edit these!!!!!!
17 % BeamEnergy = '15';
18 BeamEnergy = '6';
19 BeamQualityIndex = '0.6767';
20 % BeamQualityIndex = '0.7598';
21
22 % do not need to define excel out put file since this will be ...
   done in full
23 % sagittal m.file
24 disp('input file names')
25 toc
26 %% Get Eclipse (DICOM) Data

```

```

27 tic
28 % change directory to where the eclipse images are stored
29 originalpath = cd(filepath_dicom);
30 % make structured array of all dicom images in this directory
31 dcms=dir('*.dcm');
32 % get the names of the dicom images
33 % dcms.name
34 % re-order them correctly and make cell arrays to hold everything
35 dcms_order = zeros(1,size(dcms,1));
36 dcms_order2 = cell(1,size(dcms,1));
37 dcms_order_string = cell(1,size(dcms,1));
38 % since these aren't in the right order we take each filename, ...
    split the
39 % .dcm off the end, convert the remaining string to a number ...
    ('315'->315)
40 for q=1:size(dcms,1)
41     h=strsplit('.dcm', dcms(q).name);
42     dcms_order(1,q)=str2num(h{1});
43 end
44 % once we have all the numbers, we can sort them into the right ...
    order
45 radians=sin(dcms_order*pi/180);
46 % Becausee 90 degrees is enface, and the excel spreadsheet ...
    begins there, we
47 % must sort descending here
48 dcms_new_order=sort(radians,'descend');
49 [valuessag, iasag, ...
    ibsag]=intersect(sin(dcms_order*pi/180),dcms_new_order);
50 % since this gives us the intersecting order for each, but goes ...
    from 270 to
51 % 90 we flip the order left to right
52 dcms_order(fliplr(iasag))
53
54 % then we can put make them strings again, put the .dcm back on ...
    the ends.
55 % must use cell array for strings
56 for q=1:size(dcms_order,2)
57     dcms_order2{1,q}=num2str(dcms_order(iasag(q)));
58     g = strcat(dcms_order2{1,q}, '.dcm');
59     dcms_order_string{1,q}=g;
60 end
61 % for loop through all dcm files in directory, grabbing data in ...
    correct
62 % order
63 numdcms = size(dcms,1);
64 all_dcms = zeros(32,32,numdcms);
65 for q = 1:numdcms
66     % dcms(q).name;
67     % read in dicom image, concatenating strings to get right ...
        file name
68     filename_dicom =strcat(filepath_dicom, dcms_order_string{1,q});

```

```

69     x_uint = dicomread(filename_dicom);
70     % get header info, from which we get the dose grid scaling ...
       (since dicom
71     % put dose into grayscale and we want to go back to dose
72     xinfo = dicominfo(filename_dicom);
73     scaling = xinfo.DoseGridScaling;
74     class(scaling);
75     class(x_uint);
76     %since x_uint is an unsigned integer, we need to change the ...
       cclass to
77     %double or floating point. Otherwise, when we multiple by ...
       the scaling
78     %factor which is a double precision values, we will get very ...
       small
79     %(sub-integer numbers which Matlab would make into 0's in ...
       the array.
80     x = cast(x_uint, 'double');
81     class(x);
82     dosegrid33 = x*scaling;
83     size(dosegrid33);
84     dosegrid32 = zeros(32,32);
85     %average to get 32x32
86     for xval=1:32
87         for yval=1:32
88             dosegrid32(xval,yval) = (dosegrid33(xval,yval)+...
89             dosegrid33((xval+1),yval)+dosegrid33(xval,(yval+1))+...
90             dosegrid33((xval+1),(yval+1)))/4;
91         end
92     end
93     all_dcms(:, :, q)=dosegrid32;
94     clearvars dosegrid32 dosegrid33
95
96 end
97 % special loop needed for 90 sagittal to make orientation match ...
       matrixx
98 % orientation. Flipping the matrix to a different orientation in ...
       this case
99 % means that x1,y1 are flipped compared to dcms. We flip dcms ...
       because the
100 % cf needs to apply to the matrixx so the matrix orientation is ...
       the one we
101 % need to match
102 for z =1:size(all_dcms,3)
103     all_dcms(:, :, z)=fliplr(all_dcms(:, :, z));
104 end
105 disp('got dicom images in format required')
106 toc
107 %% Get Matrixx data
108 tic
109 % return to original matlab folder directoy which contains ...
       function files I

```

```

110 % call here and later
111 cd(originalpath)
112 % This section will take the IMRT data from excel and import the ...
    data to
113 % Matlab for analysis
114 % Find the names of the spreadsheets (contained in 'desc').
115 [typ, desc] = xlsfinfo(filename_matrixx.excel);
116 % Find the number of spreadsheets in the file
117 sheetnumber = size(desc,2);
118 % Import, giving file name, sheet name, and upper left to bottom ...
    right
119 % cells of interest (can only take a rectangular array of data).
120 % Desc holds the sheets names in a cell array, class = cell. ...
    Unfortunately
121 % 'xlsread' cannot pick out desc(1) as a string without help so ...
    we need to
122 % change the class using 'cellstr'.
123 sheet = cellstr(desc);
124 class(sheet);
125 size(sheet);
126 % Create stacked (#Dim) matrix array to hold each matrix (from ...
    each sheet).
127 IMRTarray = zeros(32,32,sheetnumber);
128 % Grab each spreadsheet in the workbook (assumes all ...
    spreadsheets have
129 % information in them that we want and we want the same cells every
130 % spreadsheet).
131 for i = 1:sheetnumber
132     IMRTarray(:, :, i) = xlsread(filename_matrixx.excel, sheet{i}, ...
        'B32:AG64');
133     %get data factor
134     [text,num]= xlsread(filename_matrixx.excel, sheet{i}, 'A16');
135     header=regexp(cast(num, 'char'), ' ', 'split');
136     scale = str2num(char(header(2)));
137     %multiply by scale, and divide to get units of gray
138     IMRTarray(:, :, i)=IMRTarray(:, :, i)*scale/1000;
139 end
140 toc
141 %% make CF table by dividing calc/meas (or eclipse/measured)
142 tic
143 % check that data is the same size from IMRT data (matrixx) and ...
    dicom
144 angles = size(all_dcms,3);
145 % if not equal, print error message
146 if size(IMRTarray,3) ≠ size(all_dcms,3)
147     disp('the number of angles for comparison do not match')
148 elseif size(IMRTarray,3) == size(all_dcms,3)
149     cf_table90 = zeros(32,32,angles);
150     for h = 1:angles
151         cf_table90(:, :, h) = all_dcms(:, :, h) ./ IMRTarray(:, :, h);
152     end

```

```

153 end
154 disp('made cf table')
155 toc
156 all_angles = fliplr([180:5:265, 266:1:274, 275:5:355,0]);
157 %% Normalize CF table to G0
158 tic
159 sx=size(cf.table90);
160 norm_cf_90sag = cf.table90./repmat(cf.table90(:, :, 1), [1 1 ...
    sx(3:end)]);
161 toc
162 % Make surface plots of CF
163 fig4=figure(4);
164 set(fig4, 'NextPlot', 'replacechildren');
165 mn_g0 = min(min(min(norm_cf_90sag)));
166 mx_g0 = max(max(max(norm_cf_90sag)));
167 axis([0 32 0 32 mn_g0 mx_g0]);
168 a=axis;
169 axis manual
170 colormap(winter)
171 for i = 1:size(norm_cf_90sag,3)
172     pause(0.5)
173     surf(norm_cf_90sag(:, :, i))
174     caxis([mn_g0 mx_g0])
175     axis(a)
176     colorbar
177     title(sheet{i})
178     zlabel('CF normalized to CF 0')
179 end
180 disp('normalized CF table to CF0 (G90)')
181 toc
182 %%
183 % clear

```

# Bibliography

- [1] Faiz M. Khan. *The Physics of Radiation Therapy*. Lippincott Williams & Wilkins, 4 edition, 2009.
- [2] Luther W. Brady Edward C. Halperin, Carlos A. Perez. *Perez and Brady's Principles and Practice of Radiation Oncology*. Lippincott Williams & Wilkins, fifth edition, 2007.
- [3] S. E. Combs, S. Konkol, D. Schulz-Ertner, M. W. Munter, J. Debus, P. E. Huber, and C. Thilmann. Intensity modulated radiotherapy (IMRT) in patients with carcinomas of the paranasal sinuses: clinical benefit for complex shaped target volumes. *Radiat Oncol*, 1:23, 2006.
- [4] KY Cheung. Intensity modulated radiotherapy: advantages, limitations and future developments. *Biomed. Imag. Intervent. J*, 2:1–19, 2006.
- [5] A. Pirzkall, M. Carol, F. Lohr, A. Hoss, M. Wannemacher, and J. Debus. Comparison of intensity-modulated radiotherapy with conventional conformal radiotherapy for complex-shaped tumors. *Int. J. Radiat. Oncol. Biol. Phys.*, 48:1371–1380, Dec 2000.
- [6] A. N. Kotte, P. Hofman, J. J. Lagendijk, M. van Vulpen, and U. A. van der Heide. Intrafraction motion of the prostate during external-beam radiation therapy: analysis of 427 patients with implanted fiducial markers. *Int. J. Radiat. Oncol. Biol. Phys.*, 69:419–425, Oct 2007.
- [7] H. Paganetti, B. S. Athar, and B. Bednarz. Dose-rate effects when estimating risks for second malignancies: in regard to Fontenot et al (Int J Radiat Oncol Biol Phys 2009;74:616-622). *Int. J. Radiat. Oncol. Biol. Phys.*, 75:1624–1625, Dec 2009.
- [8] M. Guckenberger, A. Richter, T. Krieger, J. Wilbert, K. Baier, and M. Flentje. Is a single arc sufficient in volumetric-modulated arc therapy (VMAT) for complex-shaped target volumes? *Radiother Oncol*, 93:259–265, Nov 2009.

- [9] C. X. Yu. Intensity-modulated arc therapy with dynamic multileaf collimation: an alternative to tomotherapy. *Phys Med Biol*, 40:1435–1449, Sep 1995.
- [10] Karl Otto. Volumetric modulated arc therapy: IMRT in a single gantry arc. *Medical Physics*, 35(1):310–317, 2008.
- [11] D. Palma, E. Vollans, K. James, S. Nakano, V. Moiseenko, R. Shaffer, M. McKenzie, J. Morris, and K. Otto. Volumetric modulated arc therapy for delivery of prostate radiotherapy: comparison with intensity-modulated radiotherapy and three-dimensional conformal radiotherapy. *Int. J. Radiat. Oncol. Biol. Phys.*, 72:996–1001, Nov 2008.
- [12] A. Clivio, A. Fogliata, A. Franzetti-Pellanda, G. Nicolini, E. Vanetti, R. Wyttenbach, and L. Cozzi. Volumetric-modulated arc radiotherapy for carcinomas of the anal canal: A treatment planning comparison with fixed field IMRT. *Radiother Oncol*, 92:118–124, Jul 2009.
- [13] W. F. Verbakel, J. P. Cuijpers, D. Hoffmans, M. Bieker, B. J. Slotman, and S. Senan. Volumetric intensity-modulated arc therapy vs. conventional IMRT in head-and-neck cancer: a comparative planning and dosimetric study. *Int. J. Radiat. Oncol. Biol. Phys.*, 74:252–259, May 2009.
- [14] Gary A. Ezzell, James M. Galvin, Daniel Low, Jatinder R. Palta, Isaac Rosen, Michael B. Sharpe, Ping Xia, Ying Xiao, Lei Xing, and Cedric X. Yu. Guidance document on delivery, treatment planning, and clinical implementation of IMRT: Report of the IMRT subcommittee of the AAPM radiation therapy committee. *Medical Physics*, 30(8):2089–2115, 2003.
- [15] Alan C. Hartford, Madeline G. Palisca, Thomas J. Eichler, David C. Beyer, Venkata Rao Devineni, Geoffrey S. Ibbott, Brian Kavanagh, John S. Kent, Seth A. Rosenthal, Chris J. Schultz, Prabhakar Tripuraneni, and Laurie E. Gaspar. American Society for Therapeutic Radiology and Oncology (ASTRO) and American College of Radiology (ACR) Practice Guidelines for Intensity-Modulated Radiation Therapy (IMRT). *International Journal of Radiation Oncology\*Biography\*Physics*, 73(1):9 – 14, 2009.
- [16] T. Depuydt, A. Van Esch, and D.P. Huyskens. A quantitative evaluation of IMRT dose distributions: refinement and clinical assessment of the gamma evaluation. *Radiotherapy and Oncology*, 62(3):309–319, 2002.
- [17] Daniel A. Low. Quality assurance of intensity-modulated radiotherapy. *Seminars in Radiation Oncology*, 12(3):219 – 228, 2002. Intensity-Modulated Radiation Therapy: A Clinical Perspective.

- [18] J. O'Daniel, S. Das, J. Wu, and F.F. Yin. Patient Specific Quality Assurance: Transition from IMRT to IMAT. In *Journal of Physics: Conference Series*, volume 250, page 012050. IOP Publishing, 2010.
- [19] C. Clifton Ling, Pengpeng Zhang, Yves Archambault, Jiri Bocanek, Grace Tang, and Thomas LoSasso. Commissioning and Quality Assurance of RapidArc Radiotherapy Delivery System. *International Journal of Radiation Oncology\*Biography\*Physics*, 72(2):575 – 581, 2008.
- [20] James L. Bedford and Alan P. Warrington. Commissioning of Volumetric Modulated Arc Therapy (VMAT). *International Journal of Radiation Oncology\*Biography\*Physics*, 73(2):537 – 545, 2009.
- [21] E. Schreibmann, A. Dhabaan, E. Elder, and T. Fox. Patient-specific quality assurance method for VMAT treatment delivery. *Med Phys*, 36:4530–4535, Oct 2009.
- [22] Daniel Létourneau, Julia Publicover, Jakub Kozelka, Douglas J. Moseley, and David A. Jaffray. Novel dosimetric phantom for quality assurance of volumetric modulated arc therapy. *Medical Physics*, 36(5):1813–1821, 2009.
- [23] S. Korreman, J. Medin, and F. Kjaer-Kristoffersen. Dosimetric verification of RapidArc treatment delivery. *Acta Oncol*, 48:185–191, 2009.
- [24] K. Bush, R. Townson, and S. Zavgorodni. Monte Carlo simulation of RapidArc radiotherapy delivery. *Phys Med Biol*, 53:N359–370, Oct 2008.
- [25] S. Ceberg, I. Gagne, H. Gustafsson, J. B. Scherman, S. S. Korreman, F. Kjaer-Kristoffersen, M. Hilts, and S. A. Back. RapidArc treatment verification in 3D using polymer gel dosimetry and Monte Carlo simulation. *Phys Med Biol*, 55:4885–4898, Sep 2010.
- [26] Harshad Sakhalkar, David Sterling, John Adamovics, Geoffrey Ibbott, and Mark Oldham. Investigation of the feasibility of relative 3D dosimetry in the Radiologic Physics Center Head and Neck IMRT phantom using Presage/optical-CT. *Medical Physics*, 36(7):3371–3377, 2009.
- [27] Anton Mans, Peter Remeijer, Igor Olaciregui-Ruiz, Markus Wendling, Jan-Jakob Sonke, Ben Mijnheer, Marcel van Herk, and Joep C. Stroom. 3D Dosimetric verification of volumetric-modulated arc therapy by portal dosimetry. *Radiotherapy and Oncology*, 94(2):181 – 187, 2010. Selected papers from the 10th Biennial ESTRO Conference on Physics and Radiation Technology for Clinical Radiotherapy.

- [28] IBA Dosimetry AB, Sweden. *MatriXX User's Guide*, July 2008.
- [29] L. D. Wolfsberger, M. Wagar, P. Nitsch, M. S. Bhagwat, and P. Zygmanski. Angular dose dependence of Matrixx TM and its calibration. *J Appl Clin Med Phys*, 11:3057, 2010.
- [30] IBA Dosimetry GmbH, Germany. *OmniPro I'mRT 1.7a User's Guide*, October 2005.
- [31] J Herzen, M Todorovic, F Cremers, V Platz, D Albers, A Bartels, and R Schmidt. Dosimetric evaluation of a 2D pixel ionization chamber for implementation in clinical routine. *Physics in Medicine and Biology*, 52(4):1197, 2007.
- [32] M. Donetti, E. Garelli, F. Marchetto, A. Boriani, F. Bourhaleb, R. Cirio, I. Cornelius, S. Giordanengo, A. La Rosa, U. Nastasi, and C. Peroni. A method for the inter-calibration of a matrix of sensors. *Phys Med Biol*, 51:485–495, Feb 2006.
- [33] Kwang-Ho Cheong, Sei-Kwon Kang, MeYeon Lee, Su SSan Kim, SoAh Park, Tae-Jin Hwang, Kyoung Ju Kim, Do Hoon Oh, Hoonsik Bae, and Tae-Suk Suh. Evaluation of delivered monitor unit accuracy of gated step-and-shoot IMRT using a two-dimensional detector array. *Medical Physics*, 37(3):1146–1151, 2010.
- [34] Ramesh Boggula, Friedlieb Lorenz, Lutz Mueller, Mattias Birkner, Hansjoerg Wertz, Florian Stieler, Volker Steil, Frank Lohr, and Frederik Wenz. Experimental validation of a commercial 3D dose verification system for intensity-modulated arc therapies. *Physics in Medicine and Biology*, 55(19):5619, 2010.
- [35] Richard A. Popple, John B. Fiveash, Ivan A. Brezovich, and James A. Bonner. RapidArc Radiation Therapy: First Year Experience at The University of Alabama at Birmingham. *International Journal of Radiation Oncology\*Biophysics*, In Press, Corrected Proof:–, 2010.
- [36] Barbara Dobler, Natalia Streck, Elisabeth Klein, Rainer Loeschel, Petra Haertl, and Oliver Koelbl. Hybrid plan verification for intensity-modulated radiation therapy (IMRT) using the 2D ionization chamber array I'mRT MatriXXa feasibility study. *Physics in Medicine and Biology*, 55(2):N39, 2010.
- [37] Min Rao, Wensha Yang, Fan Chen, Ke Sheng, Jinsong Ye, Vivek Mehta, David Shepard, and Daliang Cao. Comparison of Elekta VMAT with helical tomotherapy and fixed field IMRT: Plan quality, delivery efficiency and accuracy. *Medical Physics*, 37(3):1350–1359, 2010.